

# Global Biogeochemical Cycles<sup>®</sup>



## RESEARCH ARTICLE

10.1029/2024GB008398

### Key Points:

- Adaptation and acclimation of photosynthesis to temperature and CO<sub>2</sub> increases modeled global gross primary productivity (GPP) by 2050 under an RCP8.5 climate scenario
- Temperature acclimation in the extratropics enhances GPP but adaptation in the tropics weakens the CO<sub>2</sub> fertilization response decreasing GPP
- CO<sub>2</sub> acclimation down-regulates photosynthetic capacity causing a universal decline in the rate of GPP enhancement across biomes

### Supporting Information:

Supporting Information may be found in the online version of this article.

### Correspondence to:

R. J. Oliver,  
rju@ceh.ac.uk

### Citation:

Oliver, R. J., Mercado, L. M., Medlyn, B. E., Harris, P. P., & Clark, D. B. (2025). Contrasting impacts of acclimation and adaptation of photosynthetic capacity to temperature and CO<sub>2</sub> across biomes. *Global Biogeochemical Cycles*, 39, e2024GB008398. <https://doi.org/10.1029/2024GB008398>

Received 16 OCT 2024

Accepted 25 JUN 2025

### Author Contributions:

**Conceptualization:** Rebecca J. Oliver, Lina M. Mercado, Belinda E. Medlyn, Phil P. Harris

**Data curation:** Rebecca J. Oliver

**Formal analysis:** Rebecca J. Oliver

**Investigation:** Rebecca J. Oliver, Lina M. Mercado, Belinda E. Medlyn, Phil P. Harris

**Methodology:** Rebecca J. Oliver, Lina M. Mercado, Belinda E. Medlyn, Phil P. Harris, Douglas B. Clark

**Software:** Rebecca J. Oliver, Lina M. Mercado, Douglas B. Clark

**Visualization:** Rebecca J. Oliver

© 2025. The Author(s).

This is an open access article under the terms of the [Creative Commons Attribution License](#), which permits use, distribution and reproduction in any medium, provided the original work is properly cited.

## Contrasting Impacts of Acclimation and Adaptation of Photosynthetic Capacity to Temperature and CO<sub>2</sub> Across Biomes

Rebecca J. Oliver<sup>1</sup> , Lina M. Mercado<sup>1,2</sup> , Belinda E. Medlyn<sup>3</sup> , Phil P. Harris<sup>1</sup> , and Douglas B. Clark<sup>1</sup> 

<sup>1</sup>UK Centre for Ecology and Hydrology, Wallingford, UK, <sup>2</sup>University of Exeter, Exeter, UK, <sup>3</sup>Western Sydney University, Penrith, NSW, Australia

**Abstract** The response of photosynthesis to temperature and CO<sub>2</sub> is poorly represented in land surface models, contributing uncertainty to estimates of the land carbon sink. We assess the sensitivity of carbon uptake to temperature adaptation and acclimation of photosynthetic capacity and CO<sub>2</sub> acclimation of photosynthesis in the JULES model forced with an RCP8.5 climate scenario. Simulations show enhanced global gross primary productivity (GPP) when these processes are included, but over time the enhancement of GPP is weakened. In extratropical regions, temperature acclimation enhances GPP by aligning the photosynthetic temperature optimum with seasonal temperatures, allowing higher rates of carbon assimilation. In the tropics, temperature adaptation weakens the rate of global carbon uptake by reducing the CO<sub>2</sub> sensitivity of photosynthesis and limiting the CO<sub>2</sub> fertilization response, while acclimation sustains higher rates of photosynthesis as temperatures rise. Combined, our results suggest enhanced thermal resilience of modeled global GPP to warming. Downregulation of photosynthetic capacity in response to elevated CO<sub>2</sub> could substantially affect future GPP. However, this response remains uncertain, highlighting the need for improved understanding and representation of CO<sub>2</sub> acclimation across biomes, especially in tropical ecosystems where field data are scarce. Results suggest models omitting these processes may underestimate global carbon uptake and ignore important spatial variability in response to climate change.

**Plain Language Summary** Forests and grasslands are natural carbon sinks for atmospheric CO<sub>2</sub> slowing the rate of climate change. Understanding the response of natural sinks to climate change is crucial to inform their efficiency in the future. Process-based land surface models are tools to aid understanding, but predictions of the terrestrial carbon cycle remain highly uncertain. We improve the modeled physiological realism of carbon uptake processes to allow the optimum temperature of photosynthesis to vary in space and time instead of remaining fixed, and photosynthetic capacity to down-regulate in response to rising CO<sub>2</sub> concentrations. Modeled global gross primary productivity (GPP) under a high emissions scenario is higher with these new processes. Adaptation of photosynthesis to warm temperatures in the tropics weakens the CO<sub>2</sub> fertilization response of photosynthesis in this region. Photosynthetic down-regulation to rising CO<sub>2</sub> causes a universal decline in GPP across biomes. Temperature acclimation in the extra-tropics, however, drives enhanced GPP by adjusting the photosynthetic temperature optimum to seasonal temperatures, resulting in higher rates of carbon uptake, and in tropical forests, temperature acclimation maintains higher rates of photosynthesis as temperatures rise. Results suggest enhanced thermal resilience of modeled GPP to rising temperatures despite a decrease in the rate of carbon uptake over time.

## 1. Introduction

Terrestrial ecosystems currently absorb ~30% of anthropogenic CO<sub>2</sub> emissions (Friedlingstein et al., 2022), slowing the growth rate of atmospheric CO<sub>2</sub>. Land surface models (LSMs), either applied independently or embedded within Earth System Models (ESMs), are the primary tools for simulating how biogeochemical cycles respond to climate change. These models are central to predicting the size and persistence of the land carbon (C) sink. However, projections of the terrestrial C cycle remain highly uncertain, with the sensitivity of photosynthesis to temperature and CO<sub>2</sub> recognized as a significant source of this uncertainty (Arora et al., 2020; Friedlingstein, Meinshausen, et al., 2014). Because photosynthesis is the largest exchange of C between the land and the atmosphere, it is a key driver of the terrestrial C sink and accurately modeling its response to environmental change is crucial (Booth et al., 2012; Rogers et al., 2017).

**Writing – original draft:** Rebecca J. Oliver  
**Writing – review & editing:** Rebecca J. Oliver, Lina M. Mercado, Belinda E. Medlyn, Phil P. Harris, Douglas B. Clark

Photosynthesis of  $C_3$  plants is commonly modeled using the mechanistic algorithms of either Farquhar et al. (1980) or Collatz et al. (1991). These models capture the instantaneous response of C assimilation to immediate changes in environmental conditions, including temperature and  $CO_2$ , that occur on the timescale of seconds to hours. The gross rate of photosynthesis is modeled by two limiting rates determined by the photosynthetic capacity traits  $V_{cmax25}$  (the maximum rate of carboxylation at standardized temperature of 25°C) and  $J_{max25}$  (the light-saturated rate of electron transport at standardized temperature of 25°C). The instantaneous response of these physiological traits to temperature is modeled as a bell-shaped curve using an Arrhenius equation for activation plus a deactivation term (Bernacchi et al., 2001; Medlyn et al., 2002). The minimum of these two limiting rates determines the overall rate or gross photosynthesis; therefore, in response to temperature, photosynthesis follows a bell-shaped curve which peaks at the photosynthetic temperature optimum. The  $CO_2$  fertilization of photosynthesis is also captured by the Farquhar et al. (1980) model and its variants. In most LSMs, both  $V_{cmax25}$  and  $J_{max25}$  are treated as fixed parameters either by plant functional type or photosynthetic pathway. In either case, these key traits tend to be invariant in space and time in response to both temperature and  $CO_2$ . However, plants respond to environmental change on multiple timescales, and these instantaneous responses with fixed parameters miss important physiological processes such as adaptation and acclimation of photosynthetic capacity.

Many empirical studies show that the temperature optimum for photosynthesis can be adjusted through adaptation and acclimation processes as environmental conditions change. Occurring over long (multi-generational) timescales, temperature adaptation involves genetic changes in plant populations, such as modifications of photosynthetic machinery that affect enzyme structure or membrane composition, to optimize photosynthetic function for a specific temperature regime (Berry & Bjorkman, 1980). Empirical studies show that temperature responses of plant photosynthesis vary geographically, suggesting genetic adaptation of species to their local growth environment (Berry & Bjorkman, 1980; Gunderson et al., 2010). In contrast, temperature acclimation refers to shorter-term, reversible physiological adjustments that allow plants to maintain performance in response to immediate changes in environmental conditions. These may involve changes in photosynthetic enzyme activity or abundance in response to seasonal temperature fluctuations. Evidence for acclimation has been documented globally, from boreal (Benomar et al., 2017; Dusenge et al., 2020; Kroner & Way, 2016; Kurepin et al., 2018; Reich et al., 2018), to temperate (Drake et al., 2015; Guha et al., 2018; Hikosaka et al., 2007; Sendall et al., 2015), and tropical ecosystems (Carter et al., 2020; Cox et al., 2023; Dusenge et al., 2020; Slot & Winter, 2017). Furthermore, a number of studies have demonstrated that such variation in the temperature optimum for photosynthesis arises from adjustment of the photosynthetic capacity parameters  $V_{cmax25}$  and  $J_{max25}$  and their ratio to prolonged changes in temperature, showing lower values with warming (Crous et al., 2022; Kattge & Knorr, 2007; Kumarathunge et al., 2019). This provides a meaningful way to translate temperature adaptation and/or acclimation processes into LSMs.

The early work of Kattge and Knorr (2007) provided an empirical approach to represent temperature acclimation of photosynthetic capacity in LSMs (Lombardozi et al., 2015; Mercado et al., 2018; Oliver et al., 2022; Smith et al., 2016). Alternative modeling approaches beginning to emerge employ optimality-based methods within LSMs (Mengoli et al., 2022; Ren et al., 2025). However, recently, the work of Kumarathunge et al. (2019) updated the earlier empirical approach of Kattge and Knorr (2007) by directly separating the relative contribution of adaptation and acclimation to the overall observed temperature sensitivity of photosynthesis. Furthermore, the study uses a broader global database that includes more tropical species that were previously underrepresented. Therefore, the empirical relationships developed by Kumarathunge et al. (2019) currently represent the latest physiological understanding of the temperature response of photosynthetic capacity and have recently been implemented into the CABLE-POP model (Bennett et al., 2024; Knauer et al., 2023). The Kumarathunge et al. (2019) formulation shows that the observed global variation in the temperature optimum of photosynthesis arises from adaptation and/or acclimation to the temperature of  $V_{cmax25}$ ,  $J_{max25}$ , and their ratio at 25°C ( $J_{max25} : V_{cmax25}$ ). Importantly, this ratio determines the point at which photosynthesis transitions between limitation by Rubisco carboxylation capacity and limitation by electron transport. The  $J_{max25} : V_{cmax25}$  ratio declined with increasing temperature, shifting the transition between Rubisco-limited and electron transport limited photosynthesis. Because the latter rate of C assimilation is much less sensitive to  $CO_2$ , a dynamic  $J_{max25} : V_{cmax25}$  ratio will likely affect the  $CO_2$  fertilization response of vegetation. Therefore, temperature adaptation/acclimation has the potential to affect both the magnitude, and the temporal dynamics of global C uptake with climate change.

This is important to explore given the potential impact on land-atmosphere feedbacks and future climate projections.

Modeling studies show a substantial effect of photosynthetic temperature acclimation on global C uptake and future C storage, but results vary widely by region, highlighting significant uncertainties between LSMs (Bennett et al., 2024; Knauer et al., 2023; Lombardozzi et al., 2015; Mercado et al., 2018; Oliver et al., 2022; Smith et al., 2016). For example, some models predict reduced tropical C storage with temperature acclimation (Lombardozzi et al., 2015; Smith et al., 2016), while others report enhanced uptake (Bennett et al., 2024; Knauer et al., 2023; Mercado et al., 2018; Oliver et al., 2022). However, comparison among studies is difficult due to different interpretations and implementations of temperature adaptation/acclimation schemes, especially treatment of acclimation of the  $J_{max25}/V_{cmax25}$  ratio, the definition of the control simulation and different metrics used to describe the effect.

The advances made by Kumarathunge et al. (2019) are important because understanding the relative contributions of temperature adaptation and acclimation to C uptake is crucial, given that these processes operate on different timescales. Mercado et al. (2018) made an initial attempt to separate and quantify these effects on the C cycle in the JULES LSM. Adaptation was represented in the model as spatial variation in the photosynthetic capacity parameters according to a historical long-term mean growth temperature, and acclimation using the empirical scheme of Kattge and Knorr (2007). Compared with a control simulation in which all plants had the same temperature response, the study found that adaptation had twice the effect of acclimation on enhancing future land C storage, with distinct spatial patterns.

Long-term exposure to elevated atmospheric CO<sub>2</sub> (eCO<sub>2</sub>) often results in down-regulation of photosynthetic capacity. While short-term (weeks to months) eCO<sub>2</sub> experiments often show enhanced photosynthesis, many longer-term studies (years to decades) report down-regulation of  $V_{cmax}$  and  $J_{max}$  (Ainsworth & Rogers, 2007; Medlyn et al., 1999; Smith & Keenan, 2020; Yang et al., 2020), although see (Gardner et al., 2021). As leaf N is often seen to decrease, it is suggested  $V_{cmax}$  and  $J_{max}$  might decrease as a result of N dilution (Ainsworth et al., 2004; Leakey et al., 2009) or soil N limitation (Medlyn et al., 1999). Alternatively, Smith and Keenan (2020) suggest that reduced  $V_{cmax}$  under eCO<sub>2</sub> may result from photosynthetic acclimation, reflecting optimized resource investment, rather than N limitation, hypothetically releasing N to invest in other potentially limiting growth processes. Given that a large amount of leaf N is required to maintain photosynthetic machinery, some coupled C-N LSMs simulate photosynthetic capacity as a function of leaf N (Haverd et al., 2018; Lawrence et al., 2019; Rogers et al., 2017). In models where the relationship is dynamic and leaf-N responds to soil-N uptake and allocation, this indirect approach to CO<sub>2</sub> acclimation can lead to C assimilation becoming increasingly N-limited under eCO<sub>2</sub> due to lower simulated leaf N concentrations (Wieder et al., 2015). Alternatively, Smith et al. (2024) used an optimality approach to model photosynthetic CO<sub>2</sub> acclimation, allowing excess leaf N from the down-regulation of  $V_{cmax}$  to be re-distributed to other growth tissues. As a result, the simulated impact of N-limitation on biomass production under eCO<sub>2</sub> was reduced (Smith et al., 2024). However, optimality-based approaches within LSMs are only beginning to emerge and require robust testing of assumptions. Therefore, although the CO<sub>2</sub> fertilization response of photosynthesis is captured by LSMs that use a mechanistic model of photosynthesis such as Farquhar et al. (1980) or Collatz et al. (1991), the acclimation and down-regulation of photosynthetic capacity is generally not explicitly accounted for (Rogers et al., 2017).

In this study, we bring together, in one modeling framework, an improved representation of temperature adaptation and acclimation of photosynthetic capacity together with an explicit representation of CO<sub>2</sub> acclimation. We implement adaptation and acclimation of photosynthetic capacity to temperature from Kumarathunge et al. (2019) into the JULES land surface model (Joint UK Land Environment Simulator). This then allows the photosynthetic temperature optimum to vary spatially and temporally. In the model, adaptation is represented by spatial variation of the photosynthetic capacity parameters according to the historical long-term mean temperature of the growth environment. The assumption is that adaptation occurs on time-scales longer than the length of our simulation and does not vary temporally. Temperature acclimation is implemented by short-term (within season) adjustment of the photosynthetic capacity parameters in response to changes in growth temperature. CO<sub>2</sub> acclimation is represented by a decline in the  $J_{max}:V_{cmax}$  ratio with rising CO<sub>2</sub> based on results from meta-analysis data. We force JULES using a high emission RCP8.5-SSP5 climate change

**Table 1**  
Description of the JULES Model Simulation Configurations

Model Configuration	Temperature adaptation	Temperature acclimation	CO <sub>2</sub> acclimation	Description
<i>Ctl</i>	–	–	–	This represents a global adaptation baseline. Whilst photosynthetic capacity is adapted to an area-weighted global mean home temperature ( $T_{homeGB}$ ), there is no spatial (adaptation) or temporal variation (acclimation) of photosynthetic capacity to temperature. The temperature sensitivity of photosynthetic capacity for all PFTs is the same, and there is no acclimation of photosynthetic capacity to rising CO <sub>2</sub> concentration.
<i>Ad</i>	Y ( $T_{home}$ )	–	–	Temperature response of photosynthetic capacity varies spatially according to the long-term mean temperature of the home environment. This spatial variation represents inherent differences in temperature responses among plants growing in thermally contrasting habitats having adjusted leaf physiology and biochemistry over long (evolutionary) timescales to geographical variations in temperature.
<i>AdAc</i>	Y ( $T_{home}$ )	Y ( $T_{growth}$ )	–	Temperature response of photosynthetic capacity varies according to long-term spatial variation of the temperature of the home environment (as in <i>Ad</i> ) and also according to short-term (within season) temporal variation to sustained changes in growth temperature.
<i>AdAcCO2</i>	Y ( $T_{home}$ )	Y ( $T_{growth}$ )	Y	Temperature response of photosynthetic capacity varies spatially and temporally as in <i>AdAc</i> . Acclimation of photosynthetic capacity to rising CO <sub>2</sub> assumes a linear decrease of photosynthetic capacity between 400 and 550 ppm, for all PFTs.

scenario from 1960 to 2050. We test the sensitivity of modeled gross primary productivity (GPP) to these processes and determine the relative contribution of each.

We expect that temperature adaptation/acclimation will increase modeled global GPP by 2050, whereas acclimation to CO<sub>2</sub> will decrease GPP, and the interplay between these processes will determine global C uptake by 2050 as temperatures and atmospheric CO<sub>2</sub> concentration rise concurrently. We expect CO<sub>2</sub> acclimation to impact GPP similarly across biomes; however, given the low seasonal temperature variability in the tropics, we expect a larger impact of temperature adaptation on GPP in this region. In contrast, as seasonal temperature variation is higher in the temperate and boreal regions, we expect thermal acclimation to have a greater impact on GPP. We expect that as temperatures rise, a dynamic  $J_{max}:V_{cmax}$  ratio may reduce the CO<sub>2</sub> fertilization effect over time by increasing the proportion of photosynthesis limited by electron transport, altering the temporal dynamics of C uptake.

## 2. Materials and Methods

### 2.1. Land Surface Model

We use the land surface model JULES-vn5.6 (Joint UK Land Environment Simulator at version 5.6), which is the land surface component of the UK Earth System Model (UKESM) (Sellar et al., 2019), to simulate vegetation C uptake over time in response to a changing climate. JULES simulates the exchange of water, energy and carbon between the land surface and the atmosphere. A full description of the main components of JULES is provided by Best et al. (2011) and Clark et al. (2011). Details of the representation of leaf plant physiology in JULES and scaling from leaf to canopy to grid-box are given in note S1. In this study, we run JULES with nine vegetation plant functional types (PFTs) (tropical and temperate broadleaf evergreen trees, broadleaf deciduous trees, needle-leaf evergreen and deciduous trees, C<sub>3</sub> and C<sub>4</sub> grasses, and evergreen and deciduous shrubs) with improved plant physiological parameterization as described in Harper et al. (2016). We use the recently implemented Farquhar photosynthesis scheme for C<sub>3</sub> vegetation types and the Medlyn stomatal conductance scheme described in Oliver et al. (2022). Photosynthetic temperature adaptation and acclimation is implemented using the algorithm of Kumarathunge et al. (2019) and having been developed for use with the Farquhar et al. (1980) photosynthesis scheme it is applied to just the C<sub>3</sub> PFTs in the JULES model, hence the C<sub>4</sub> grass PFT does not acclimate to temperature.

## 2.2. Implementation of Adaptation and Acclimation of Photosynthetic Capacity to Temperature and Acclimation to CO<sub>2</sub>

Four JULES model configurations are used in an additive set of simulations to determine the individual and combined effects of adaptation and acclimation to temperature and acclimation to CO<sub>2</sub>, which are described in Table 1.

We use a peaked Arrhenius function (Equation 1) to describe the instantaneous response of photosynthesis to temperature.

$$k_T = k_{25} \exp \left[ H_a \frac{(T_l - T_{ref})}{T_{ref} R T_l} \right] \frac{1 + \exp \left[ \frac{T_{ref} \Delta S - H_d}{T_{ref} R} \right]}{1 + \exp \left[ \frac{T_l \Delta S - H_d}{T_l R} \right]} \quad (1)$$

where,  $k_T$  ( $\mu\text{mol m}^2 \text{s}^{-1}$ ) is either  $V_{cmax}$  or  $J_{max}$  at leaf temperature  $T_l$  (K),  $k_{25}$  ( $\mu\text{mol m}^2 \text{s}^{-1}$ ) is the rate of  $V_{cmax}$  or  $J_{max}$  at the reference temperature  $T_{ref}$  of 25°C (298.15 K),  $R$  is the universal gas constant ( $8.314 \text{ J mol}^{-1} \text{ K}^{-1}$ ),  $H_a$  and  $H_d$  ( $\text{J mol}^{-1}$ ) are the activation and deactivation energies, respectively, and  $\Delta S$  ( $\text{J mol}^{-1} \text{ K}^{-1}$ ) is an entropy term.  $H_d$  is fixed at  $200,000 \text{ J mol}^{-1}$  as in Kumarathunge et al. (2019).

To represent adaptation and acclimation of photosynthetic capacity to temperature for C<sub>3</sub> vegetation, Kumarathunge et al. (2019) developed four global empirical functions that modify Equation 1 to account for the enzymatic response of  $V_{cmax}$  and  $J_{max}$  to temperature. These functions use home temperature ( $T_{home}$ ) to account for adaptation, defined as the mean (1970–2000) maximum air temperature of the warmest month at the species seed source, and growth temperature ( $T_{growth}$ ) to account for acclimation, defined as the mean air temperature of the previous 30 days. In JULES  $T_{growth}$  is calculated using an exponential weighted moving average with a decay constant of 30 days. This avoids the computational cost of storing time step data associated with a simple 30-day moving average.  $T_{home}$  does not change in time as this reflects the long-term historical temperature conditions to which the vegetation has adapted at the start of the simulation. Kumarathunge et al. (2019) found that the observed global variation in the optimum temperature for photosynthesis ( $T_{optA}$ ) was explained by the effect of  $T_{growth}$  alone on both the activation energy ( $H_{aV}$ ) and the entropy term ( $\Delta S_V$ ) of  $V_{cmax}$ , and both  $T_{growth}$  and  $T_{home}$  on the entropy term of  $J_{max}$  ( $\Delta S_J$ ) and the ratio of  $J_{max}$  to  $V_{cmax}$  at 25°C ( $J_{max25} \cdot V_{cmax25}$ ).

For the implementation of adaptation and acclimation to temperature into JULES (configuration *AdAc*, Table 1),  $H_a$  and  $\Delta S$  in Equation 1 become functions of either  $T_{growth}$  alone (Equation 2,  $H_{aV}$  and  $\Delta S_V$ ), or both  $T_{growth}$  and  $T_{home}$  (Equation 3,  $\Delta S_J$  and  $J_{max25} \cdot V_{cmax25}$ ). A global constant is used for  $H_{dJ}$  as in the study of (Kumarathunge et al., 2019):

$$f(T_{growth}) = A_{ac} + \alpha_{ac} T_{growth} \quad (2)$$

$$f(T_{home}, T_{growth}) = A_{ad} + \alpha_{ad} T_{home} + \delta_{ac} (T_{growth} - T_{home}) \quad (3)$$

where,  $A_{ac}$  is the parameter when  $T_{growth} = 0$ ,  $A_{ad}$  is the parameter when  $T_{home} = 0$ ,  $\alpha_{ac}$  is the acclimation coefficient ( $^{\circ}\text{C}^{-1}$ ),  $\alpha_{ad}$  is the adaptation coefficient ( $^{\circ}\text{C}^{-1}$ ) and  $\delta_{ac}$  is the acclimation coefficient corresponding to a unit deviation in  $T_{growth}$  from  $T_{home}$  ( $^{\circ}\text{C}^{-1}$ ). Table S1 in Supporting Information S1 shows the parameter values used for these functions taken from the global analysis of Kumarathunge et al. (2019). According to these relationships, the optimum temperature of  $V_{cmax}$  ( $T_{optV}$ ) increases by  $0.71 \pm 0.2^{\circ}\text{C } ^{\circ}\text{C}^{-1}$  increase in  $T_{growth}$ , and the optimum temperature of  $J_{max}$  ( $T_{optJ}$ ) increases by  $0.63 \pm 0.15^{\circ}\text{C } ^{\circ}\text{C}^{-1}$ .

Our implementation of the acclimated  $J_{max25} \cdot V_{cmax25}$  ratio to determine  $J_{max25}$  follows Mercado et al. (2018), in which both  $J_{max25}$  and  $V_{cmax25}$  are modified by  $T_{growth}$  under the assumption that the total amount of leaf N allocated to photosynthesis remains constant, but leaf N is allocated between  $J_{max25}$  and  $V_{cmax25}$  at a fixed ratio of 5.3:3.8 according to observations (Medlyn, 1996). Therefore, decreasing  $J_{max25}$  increases  $V_{cmax25}$  to maintain the balance between the N requirements of both processes. We acknowledge that the assumption of a fixed ratio of nitrogen allocation simplifies the complex reality. Numerous studies demonstrate that plants can dynamically adjust the relative proportions of  $J_{max25}$  and  $V_{cmax25}$  in response to various environmental factors, including light availability, nutrient status, and leaf morphology (Domingues et al., 2010; Evans & Poorter, 2001; Walker

et al., 2014). However, this approach aims to simplistically capture the idea of resource use optimization (Walker et al., 2014), and we consider this a more physiologically realistic approach than adjusting  $J_{max25}$  alone in response to temperature.

We explore the impact of adaptation to temperature alone (configuration *Ad*, Table 1) by using the adaptation components of the Kumarathunge et al. (2019) scheme to modify parameters according to  $T_{home}$  (Equation 4; Table S1 in Supporting Information S1).

$$f(T_{home}) = A_{ad} + \alpha_{ad}T_{home} \quad (4)$$

The impact of thermal acclimation alone is explored as the difference between configurations *AdAc-Ad*.

Our baseline *Ctl* (Table 1) simulation represents a “global adaptation baseline” in which photosynthetic capacity (i.e.,  $V_{cmax}$  and  $J_{max}$ ) in all  $C_3$  vegetation has the same temperature sensitivity, and there is no spatial or temporal variation. We use an area-weighted global mean home temperature ( $T_{homeGB}$ , 24.26°C, Table S1 in Supporting Information S1) calculated as the annual mean maximum air temperature in the tropics, and the mean maximum air temperature of the three months with the highest NDVI elsewhere over the period 1970 to 2000 from the WorldClim-2.1 data set (Note S2). The global  $T_{homeGB}$  is used to derive parameter values for the temperature response of  $V_{cmax}$  and  $J_{max}$  and the  $J_{max25}:V_{cmax25}$  ratio using the adaptation components (Equation 4) from the algorithm of Kumarathunge et al. (2019) (Table S1 in Supporting Information S1). Note S2 describes the calculation of  $T_{growth}$ ,  $T_{home}$  and the global  $T_{homeGB}$ .

Acclimation of photosynthetic capacity to  $eCO_2$  (*AdAcCO2*, Table 1) is implemented based on observations from large meta-analyses (Ainsworth & Rogers, 2007; Medlyn et al., 1999; Smith & Keenan, 2020) that suggest  $V_{cmax}$  and  $J_{max}$  down-regulate with increasing  $CO_2$  concentration (Table S2 in Supporting Information S1). These studies together suggest that in elevated  $CO_2$   $V_{cmax}$  decreases by ~10% and  $J_{max}$  decreases by ~3.5%, and the  $J_{max25}:V_{cmax25}$  ratio increases. Our study provides an initial assessment of the sensitivity of photosynthesis to  $CO_2$  acclimation. Therefore, in the absence of greater understanding of the mechanisms behind this process, we derived Equations 5 and 6 below so that once the atmospheric  $CO_2$  concentration is above 400 ppm, both  $V_{cmax}$  and  $J_{max}$  decline linearly until 500 ppm. Once atmospheric  $CO_2$  concentration has reached 500 ppm,  $V_{cmax}$  has decreased by ~10% and  $J_{max}$  has decreased by ~3.5%, and the  $J_{max}:V_{cmax}$  ratio has increased.

$$V_{cmaxco2} = V_{cmax}((-0.0007)c_a + 1.28) \quad (5)$$

$$J_{maxco2} = J_{max}((-0.000208)c_a + 1.08) \quad (6)$$

where,  $V_{cmax}$  and  $J_{max}$  are the values adjusted to temperature, and  $c_a$  (ppm) is the atmospheric  $CO_2$  concentration (ppm).

### 2.3. Global Simulations

Global simulations with JULES are driven with meteorological output (1960–2050) from a HadGEM3-GC3.1 model simulation that follows the CMIP6 modeling protocol and is based on a non-mitigation SSP5 pathway and high-emissions RCP8.5 scenario (Haarsma et al., 2016; Roberts et al., 2019; Williams et al., 2018). The meteorological forcing data was re-gridded to  $0.5^\circ \times 0.5^\circ$  and is on an hourly model timestep. Figure S2 in Supporting Information S1 shows timeseries of annual mean temperature and precipitation by region over the study period, and the atmospheric  $CO_2$  concentration. To isolate the direct effects of adaptation and acclimation to temperature and  $CO_2$  on GPP, the land surface properties of the model were prescribed. Therefore, we use a static map of land cover fraction in each grid-cell derived from the ESA LC\_CCI global vegetation distribution version 1.6 for the year 2010 (Poulter et al., 2015) (Figure S3 in Supporting Information S1), and seasonally varying *LAI* derived from the Global Land Surface Satellite (GLASS) data set (Xiao et al., 2016). A spin-up of 80 years (re-cycling through the period 1960 to 1980) was sufficient to equilibrate soil temperature and soil moisture. To understand the global trends, we break down the results by latitude bands to explore responses within different biomes.

## 2.4. Leaf-Level Simulations

To help understand the global simulations, the temperature response of light-saturated gross photosynthesis for top of canopy sunlit leaves was simulated for each model configuration at three grid-cells to cover vegetation types typical of the tropical (broadleaf evergreen tropical tree; grid-cell 4.75°S, 61.25°W), temperate ( $C_3$  grass; grid-cell 52.75°N, 24.75°E) and boreal (needle leaf evergreen tree; grid-cell 61.25°N, 14.25°E) regions according to a land cover map used in the global simulations. Mean conditions in 1960 and 2050 (atmospheric  $CO_2$  concentration, mean daytime leaf temperature and mean  $T_{growth}$ ) are calculated from the relevant data sets used in, or output generated by, the global simulations for the corresponding grid-cell. In this leaf-level model, simplification is used to calculate the intercellular  $CO_2$  concentration ( $c_i$ ), which is assumed to maintain the ratio  $c_i/c_a = 0.7$ .

## 2.5. Model Evaluation

Site-level simulations for the *Ctl*, *Ad* and *AdAc* configurations at 10 eddy covariance flux-sites were performed for evaluation of simulated GPP fluxes against observed seasonal cycles of GPP. Additionally, we ran global scale present-day simulations (1979–2013) for *Ctl*, *Ad* and *AdAc* configurations at  $0.5^\circ \times 0.5^\circ$  resolution and hourly model timestep forcing JULES with observed meteorology from the WATCH forcing data set using ERA-Interim reanalysis (WFDEI) for evaluation of seasonal mean simulated GPP against observational products. These simulations are described in Note S3, and evaluation is shown in Figures S4 and S5 in Supporting Information S1.

## 2.6. Postprocessing

Our target variable of interest is the change in GPP over the simulation period from 1960 to 2050 that we refer to as  $dGPP$ . To determine the change in the rate of GPP over time caused by a particular model process and taking into account the different starting points of the simulations, the difference in  $dGPP$  between pairs of simulations is calculated as in Equation 7, where the GPP at the start of the simulation is the decadal mean over 1960 to 1970 (referred to as  $GPP_{1970}$ ) and the GPP at the end of the simulation is the mean over 2040 to 2050 (referred to as  $GPP_{2050}$ ), and  $a$  and  $b$  refer to different model configurations. For example,  $(dGPP_{AdAc}) - (dGPP_{Ad})$  isolates the effect of acclimation to temperature on GPP; whilst  $dGPP$  for each simulation gives the change in GPP over time, the difference between these quantifies how acclimation to temperature changes  $dGPP$  relative to the change caused by adaptation to temperature. To determine the effect of adaptation to temperature,  $a$  and  $b$  in Equation 7 denote *Ad* and *Ctl*, respectively. To determine the effect of acclimation to  $CO_2$ ,  $a$  and  $b$  denote *AdAcCO2* and *AdAc*, respectively. The combined effect of adaptation and acclimation to temperature is determined where  $a$  and  $b$  are *AdAc* and *Ctl*, respectively, and the effect of all processes together is determined where  $a$  and  $b$  are *AdAcCO2* and *Ctl*, respectively. Equation 8 estimates the percentage change due to the different process effects.

$$Effect = (\overline{GPP}_{a_{2050}} - \overline{GPP}_{a_{1970}}) - (\overline{GPP}_{b_{2050}} - \overline{GPP}_{b_{1970}}) \quad (7)$$

$$Effect(\%) = \left( \frac{(\overline{GPP}_{a_{2050}} - \overline{GPP}_{a_{1970}}) - (\overline{GPP}_{b_{2050}} - \overline{GPP}_{b_{1970}})}{(\overline{GPP}_{b_{2050}} - \overline{GPP}_{b_{1970}})} \right) \times 100 \quad (8)$$

## 3. Results

### 3.1. Global Analysis of GPP Change Into the Future

Simulated mean annual global GPP is higher under all model configurations compared to the baseline *Ctl* throughout the study period (Figure 1a, Table 2). However, the rate of change in GPP over time is reduced leading to a lower overall change in GPP from 1970 to 2050 ( $dGPP$ ) under all new model configurations (Table 2).

At the global scale, when isolating the individual effects of each process (Equations 7 and 8), adaptation to temperature enhances simulated GPP, but this enhancement weakens over the study period with  $dGPP$  being 1.9  $PgC\ yr^{-1}$  (5.8%) lower in *Ad* than in *Ctl* (Figure 1b blue line, Table 3). The effect of acclimation to temperature alone leads to a greater enhancement of mean absolute GPP in 1970 (by 2.9  $PgC\ yr^{-1}$  (acclimation) compared to 2.1  $PgC\ yr^{-1}$  (adaptation)). However, across the simulation period, acclimation to temperature has minimal effect on the rate of GPP change over time relative to adaptation (0.1  $PgC\ yr^{-1}$  (0.2%) decrease) (Figure 1b faint yellow line, Table 3). This is because the contrasting effects of acclimation to temperature in the tropics and subtropics

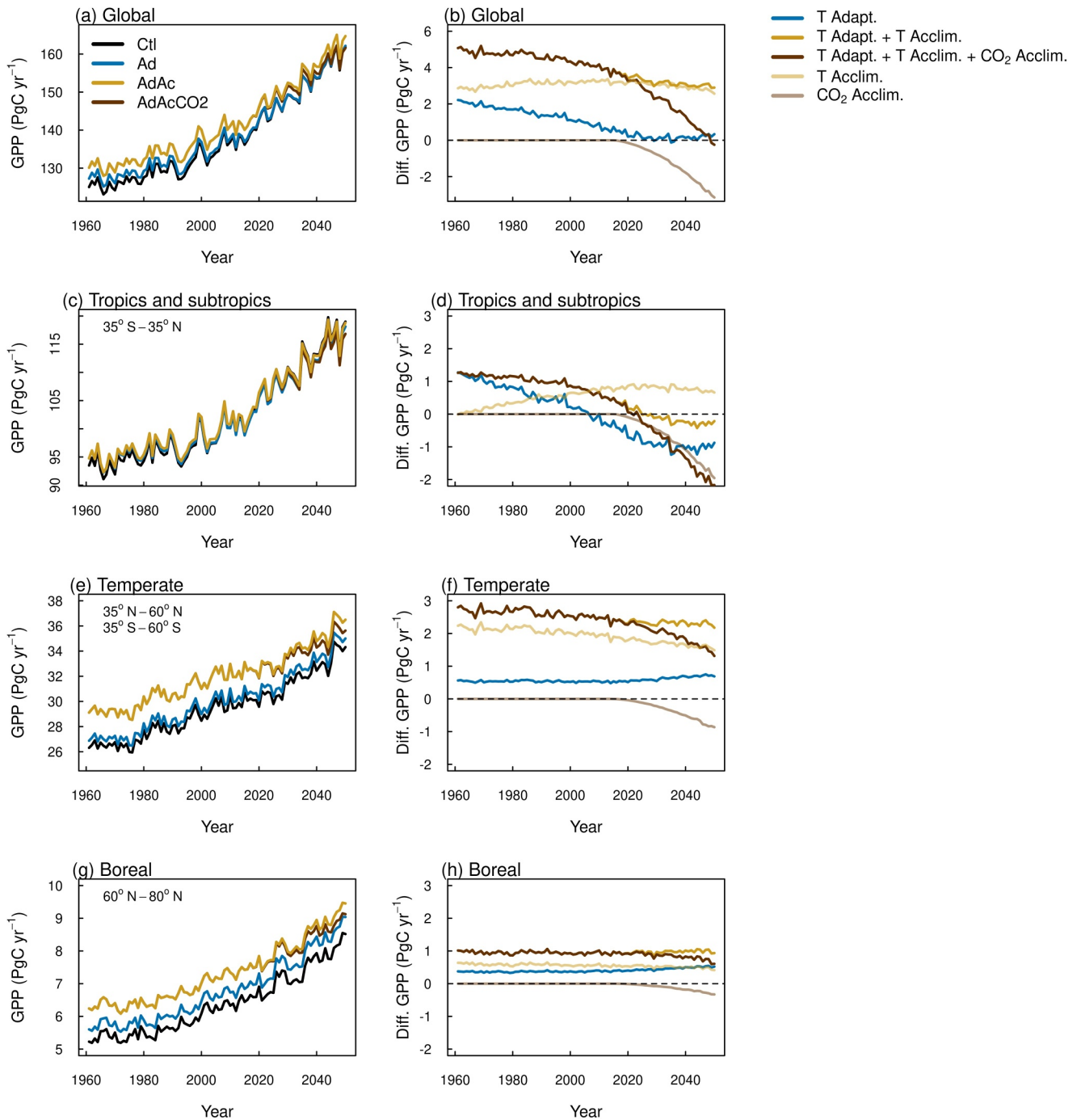


**Figure 1.** (a, c, e, and g) Time series of gross primary productivity (GPP) ( $\text{Pg C yr}^{-1}$ ) from 1960 to 2050 for the control simulation (*Ctl*), temperature adaptation (*Ad*), temperature adaptation and acclimation (*AdAc*) and temperature adaptation and acclimation with  $\text{CO}_2$  acclimation (*AdAcCO\_2*). (b, d, f, and h) the GPP difference between pairs of simulations. T Adapt. (*Ad-Ctl*) shows the effect of temperature adaptation on how GPP changes over time relative to the control simulation, T adapt. + T Acclim. (*AdAc-Ctl*) shows the effect of temperature adaptation and acclimation relative to the control, and T Adapt. + T Acclim. +  $\text{CO}_2$  Acclim. (*AdAcCO\_2-Ctl*) shows the effect of all processes together relative to the control. T Acclim. (*AdAc-Ad*) isolates the effect of temperature acclimation, and  $\text{CO}_2$  Acclim. (*AdAcCO\_2-AdAc*) isolates the effect of  $\text{CO}_2$  acclimation.

(increased rate of GPP change) compared to the temperate and boreal regions (reduced rate of GPP change) almost completely cancel out the effect at the global scale (Table 3); the reasons for these contrasting effects are discussed later. Therefore, globally, while the effect of acclimation to temperature enhances mean GPP, it does little to alleviate the slowdown in GPP change over time. Consequently, in combination, *AdAc* results in a similar

**Table 2**  
Simulated Mean Gross Primary Productivity (GPP) by Region and Globally in 1970 (1960–1970 Mean) and 2050 (2040–2050 Mean), and the Change Over Time (*d*GPP Expressed as %) for Each Model Configuration

	GPP (Pg C yr <sup>-1</sup> ) and % difference											
	Tropics and subtropics			Temperate			Boreal			Global		
	1970	2050	<i>d</i> GPP %	1970	2050	<i>d</i> GPP %	1970	2050	<i>d</i> GPP %	1970	2050	<i>d</i> GPP %
<i>Ctl</i>	93.1	116.4	25.0	26.7	33.5	25.5	5.4	8.0	48.1	125.2	157.9	26.1
<i>Ad</i>	94.3	115.4	22.4	27.2	34.1	25.4	5.8	8.5	46.6	127.3	158.1	24.2
<i>AdAc</i>	94.4	116.1	23.0	29.4	35.8	21.8	6.4	9.0	40.6	130.2	160.9	23.6
<i>AdAcCO2</i>	94.4	114.6	21.4	29.4	35.1	19.4	6.4	8.8	37.5	130.2	158.5	21.7

weakening of GPP over the simulation period to *Ad* (Figure 1b bold yellow line, Table 3). Acclimation to CO<sub>2</sub> alone decreased *d*GPP relative to *AdAc* by 2.4 PgC yr<sup>-1</sup> (8.0% decrease) (Figure 1b faint brown line, Table 3). The decrease in *d*GPP occurs from year 2020 onwards as prescribed in our parameterization. The effect of all processes together is additive, therefore *AdAcCO2* decreases the rate of C uptake globally over the simulation period with *d*GPP being 4.4 PgC yr<sup>-1</sup> (13.5%) lower in *AdAcCO2* than in *Ctl* (Figure 1b bold brown line, Table 3) and results in the largest change (decrease) in *d*GPP.

### 3.2. Regional Analysis of GPP Change and Underlying Mechanisms

In the tropics and subtropics, the effect of adaptation to temperature dominates at the start of the simulation to drive a large increase in absolute GPP above *Ctl* (1.2 PgC yr<sup>-1</sup> higher) (Table 2, Figure S11 in Supporting Information S1 for spatial patterns). However, over the course of the simulation period this enhancement is weakened so *d*GPP is 2.2 PgC yr<sup>-1</sup> (9.4%) lower in *Ad* compared to *Ctl* (Table 3), leading to lower mean annual GPP in 2050 in this simulation setup compared to *Ctl* (Figure 1d, Table 2, Figure S11 in Supporting Information S1). It is this adaptation response to temperature in the tropics and subtropics that drives the long-term global trend of weakening C uptake over time relative to our *Ctl* simulation (Figures 1b and 2b). This large slowdown in the GPP trend is explained by a decrease in the photosynthetic sensitivity to CO<sub>2</sub>. The  $J_{max25}:V_{cmax25}$  ratio determines the point at which photosynthesis transitions from CO<sub>2</sub>-limited to light-limited, which is much less sensitive to increasing CO<sub>2</sub> at higher CO<sub>2</sub> concentrations. The  $J_{max25}:V_{cmax25}$  ratio decreases with increasing temperature, and the high  $T_{home}$  in this region means that the ratio in our *Ad* simulation is lower than that in *Ctl*.

**Table 3**  
The Change in Gross Primary Productivity (GPP) (*d*GPP) Over the Simulation Period (1960–2050) in Pg C yr<sup>-1</sup>, and the Change in *d*GPP Relative to a Paired Baseline Simulation, Expressed in Pg C yr<sup>-1</sup> or % Change

	Tropics + subtropics	Temperate	Boreal	Global
Change in GPP over simulation period (1970–2050):	<i>d</i> GPP (Pg C yr <sup>-1</sup> )			
<i>d</i> GPP <i>Ctl</i>	23.3	6.8	2.6	32.7
<i>d</i> GPP <i>Ad</i>	21.1	6.9	2.7	30.8
<i>d</i> GPP <i>AdAc</i>	21.7	6.4	2.6	30.7
<i>d</i> GPP <i>AdAcCO2</i>	20.2	5.7	2.4	28.3
Impact of processes on rate of GPP change:	Relative <i>d</i> GPP (Pg C yr <sup>-1</sup> (%))			
T adaptation ( <i>d</i> GPP <i>Ad</i> – <i>d</i> GPP <i>Ctl</i> )	–2.2 (–9.4)	0.1 (1.5)	0.1 (3.8)	–1.9 (–5.8)
T adaptation + T acclimation ( <i>d</i> GPP <i>AdAc</i> – <i>d</i> GPP <i>Ctl</i> )	–1.6 (–6.9)	–0.4 (–5.9)	0.0 (0.0)	–2.0 (–6.0)
T adapt. + T acclim. + CO <sub>2</sub> acclim. ( <i>d</i> GPP <i>AdAcCO2</i> – <i>d</i> GPP <i>Ctl</i> )	–3.1 (–13.3)	–1.1 (–16.2)	–0.2 (–7.7)	–4.4 (–13.5)
T acclimation ( <i>d</i> GPP <i>AdAc</i> – <i>d</i> GPP <i>Ad</i> )	0.6 (2.8)	–0.5 (–7.2)	–0.1 (–3.7)	–0.1 (–0.2)
CO <sub>2</sub> acclimation ( <i>d</i> GPP <i>AdAcCO2</i> – <i>d</i> GPP <i>AdAc</i> )	–1.5 (–6.9)	–0.7 (–10.9)	–0.2 (–7.7)	–2.4 (–8.0)

*Note.* *d*GPP is the change in mean annual GPP from 1970 (calculated as the decadal mean from 1960 to 1970 mean) to 2050 (2040 to 2050 mean). The difference in *d*GPP between pairs of simulations isolates process effects on *d*GPP independent of different starting points of simulations. It shows the rate of GPP change over time relative to a baseline simulation where negative numbers show the rate of GPP change slows over time relative to the baseline and positive number show it has increased.

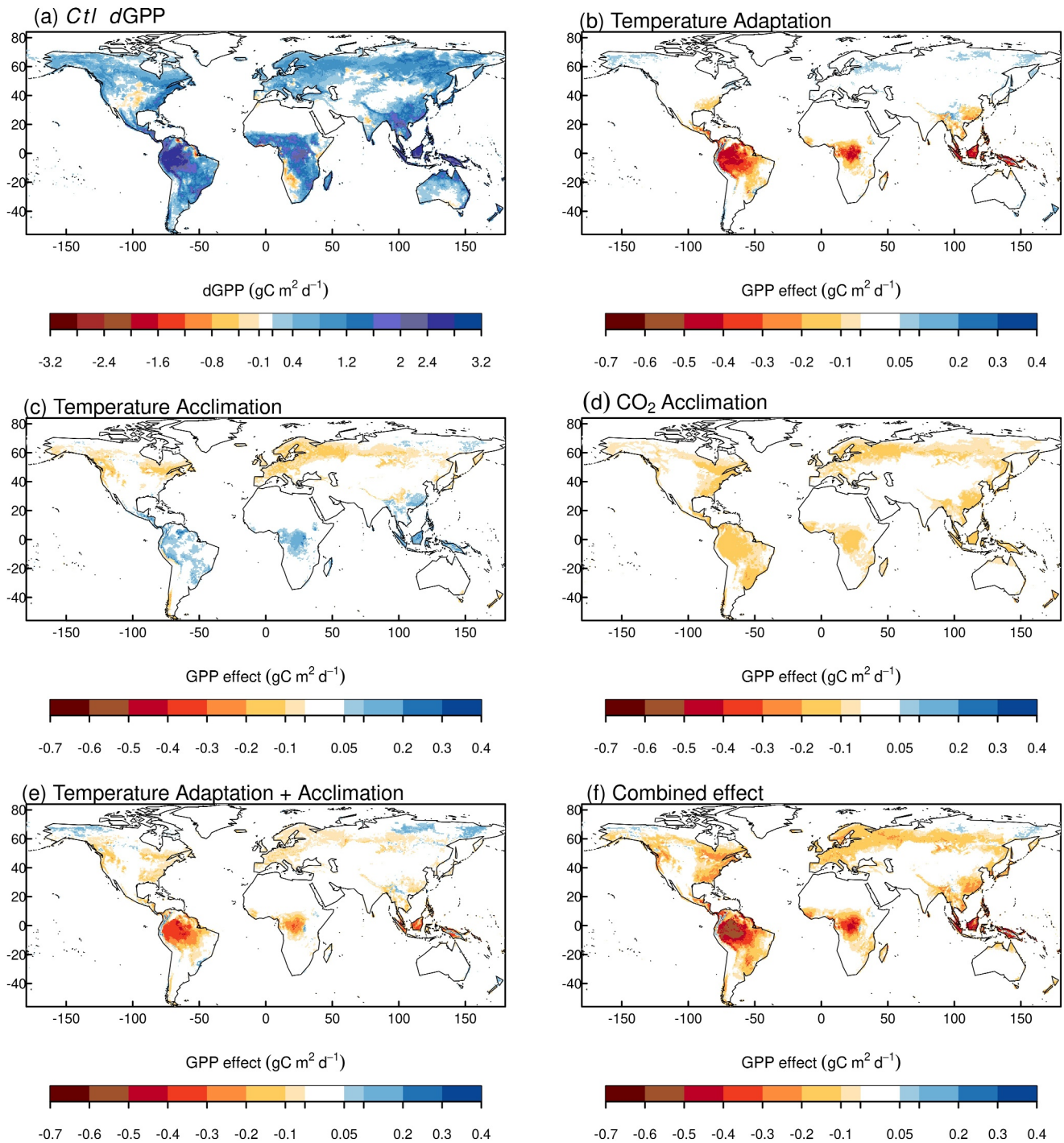


**Figure 2.** Spatial patterns of (a)  $dGPP$  ( $g\ C\ m^{-2}\ d^{-1}$ ) for the *Ctl* baseline simulation to show the change in gross primary productivity (GPP) over the simulation period from 1970 (calculated as the decadal mean over 1960 to 1970) to 2050 (2040 to 2050 mean). In (b–f) spatial patterns of the difference in  $dGPP$  between pairs of simulations (calculated using Equation 7) show the effect of individual and combined model processes on the rate of change of C uptake over time (GPP effect ( $g\ C\ m^{-2}\ d^{-1}$ )) (See Figure S15 in Supporting Information S1 for  $dGPP$  of each simulation): (b) temperature adaptation ( $dGPP\ Ad-dGPP\ Ctl$ ), (c) temperature acclimation ( $dGPP\ AdAc-dGPP\ Ad$ ), and (d)  $CO_2$  acclimation ( $dGPP\ AdAcCO_2-dGPP\ AdAc$ ), (e) temperature adaptation and acclimation ( $dGPP\ AdAc-dGPP\ Ctl$ ), and (f) all process ( $dGPP\ AdAcCO_2-dGPP\ Ctl$ ). For (b–f) reds indicate a decrease in the rate of change of GPP from 1970 to 2050 relative to the baseline simulation, and blues indicate an increase in  $dGPP$  relative to the baseline.

Lower  $J_{max25}$  means photosynthesis transitions earlier from the CO<sub>2</sub>-limited rate to the less CO<sub>2</sub> sensitive light-limited rate, and consequently the rate of C assimilation is reduced as CO<sub>2</sub> concentrations rise. The effect of temperature on the  $J_{max25}:V_{cmax25}$  ratio and its consequent impact on the transition point between CO<sub>2</sub>-limited and light-limited photosynthesis in the tropical region is shown in Figures S12 and S13 in Supporting Information S1. Our results are further illustrated with simulations in Figure S14 in Supporting Information S1 performed with a fixed 1960 atmospheric CO<sub>2</sub> concentration. These results show that the decline in  $dGPP$  with adaptation to temperature in the tropics and subtropics (and globally) disappears when the sensitivity of photosynthetic rate to CO<sub>2</sub> concentration stays the same between simulations (*Ad* and *Ctl*) (i.e., photosynthesis in all simulations at this CO<sub>2</sub> concentration are CO<sub>2</sub>-limited).

In contrast, in the tropics and subtropics, the effect of acclimation to temperature alone gradually increases over time, so  $dGPP$  is 0.6 PgC yr<sup>-1</sup> (2.8%) higher in *Ac* than in *Ad* (Figure 1d, Table 3, Figure 2c). *Ac* therefore mitigates some of the decline in the  $dGPP$  trend caused by *Ad*. This is explained by the dynamically changing  $T_{growth}$ , which is often lower than the fixed  $T_{home}$ . This increases the  $J_{max25}:V_{cmax25}$  ratio and delays the transition from CO<sub>2</sub>-limited to light-limited photosynthesis in *Ac* compared to *Ad* (Figures S12 and S13 in Supporting Information S1). Therefore, *Ac* maintains a higher CO<sub>2</sub> sensitivity of photosynthesis for longer (and higher rate of C assimilation at a given CO<sub>2</sub> concentration) compared to *Ad*. Consequently, the interaction of both adaptation and acclimation to temperature together (*AdAc*) results in a smaller decrease in the rate of C uptake from 1970 to 2050 (1.6 PgC yr<sup>-1</sup> (6.9% decrease), Table 3, Figure 2e) relative to *Ctl* than when temperature adaptation alone is considered.

In the temperate and boreal regions, adaptation to temperature has a much smaller impact on GPP (Figures 1f and 1h). In both these regions, adaptation to temperature increases mean GPP slightly (~0.5 PgC yr<sup>-1</sup>) above the *Ctl* baseline (Table 2, Figure S11 in Supporting Information S1), and relative to *Ctl* there is a slight increase in  $dGPP$  over the simulation period (0.1 PgC yr<sup>-1</sup> (1.5% increase temperate), (3.8% increase boreal), Table 3, Figure 2b). This occurs in the latter part of our simulations as CO<sub>2</sub> concentrations rapidly rise and is again due to a change in the CO<sub>2</sub> sensitivity of carbon assimilation as mediated through the  $J_{max25}:V_{cmax25}$  ratio. In the temperate and boreal regions, the  $J_{max25}:V_{cmax25}$  ratio is slightly lower in *Ctl* compared to *Ad*, which results in photosynthesis under *Ctl* being more light-limited, hence with a lower CO<sub>2</sub> sensitivity and C assimilation rate. This is illustrated in Figure S14 in Supporting Information S1, which shows this increase in  $dGPP$  in *Ad* relative to *Ctl* disappears when the atmospheric CO<sub>2</sub> concentration is fixed and photosynthetic rates in the two simulations have the same CO<sub>2</sub> sensitivity.

In contrast, acclimation to temperature causes a large increase in mean GPP relative to *Ad* in the temperate (2.2 PgC yr<sup>-1</sup> increase) and boreal (1.6 PgC yr<sup>-1</sup> increase) regions (Table 2, Figures 1f and 1h, Figure S11 in Supporting Information S1). However, the effect of acclimation to temperature alone on the GPP trend weakens over time in these regions. In the boreal region, only a slight decrease in  $dGPP$  is simulated from 1970 to 2050 (0.1 PgC yr<sup>-1</sup> (3.7% decrease)), but it is larger in the temperate region with  $dGPP$  being 0.5 PgC yr<sup>-1</sup> (7.2%) lower in *Ac* than in *Ad* (Table 3, Figure 2c). This is because of the change in the temperature sensitivity of photosynthesis in response to increasing  $T_{growth}$ . As  $T_{optA}$  under *AdAc* increases with  $T_{growth}$  it moves closer to the higher  $T_{optA}$  simulated under *Ad* and therefore decreases the difference in C assimilation rates at  $T_{leaf}$  between acclimation and adaptation to temperature (this effect can be seen in Figures 3c and 3e). Together, both adaptation and acclimation to temperature result in a large enhancement of mean GPP above the baseline *Ctl* simulation (particularly in the temperate region (2.7 PgC yr<sup>-1</sup> increase in 1970 and 2.3 PgC yr<sup>-1</sup> increase in 2050, Table 2, Figure S11 in Supporting Information S1)). In the boreal region, there is no change in  $dGPP$  over the course of the simulation because the positive and negative effects of adaptation and acclimation to temperature cancel out. However, in the temperate region, a more substantial decrease in  $dGPP$  is simulated, which is 0.4 PgC yr<sup>-1</sup> (5.9%) lower in *AdAc* than in *Ctl* because of the stronger effect acclimation to temperature has on weakening the uptake of C over time (Table 3, Figure 2e). It is therefore acclimation to temperature in these regions that dominates the enhancement of GPP above the *Ctl* baseline at the global scale.

Across all regions, acclimation to CO<sub>2</sub> causes a large decrease in  $dGPP$  relative to *AdAc* (tropics and subtropics: 1.5 PgC yr<sup>-1</sup> (6.9% decrease), temperate: 0.7 PgC yr<sup>-1</sup> (10.9% decrease), boreal: 0.2 PgC yr<sup>-1</sup> (7.7% decrease), Table 3, Figure 2d). Therefore, with all processes combined, in all regions, *AdAcCO2* results in the largest slowdown of the GPP trend over time. In the tropics and subtropics,  $dGPP$  is 3.1 PgC yr<sup>-1</sup> (13.3%) lower, in the

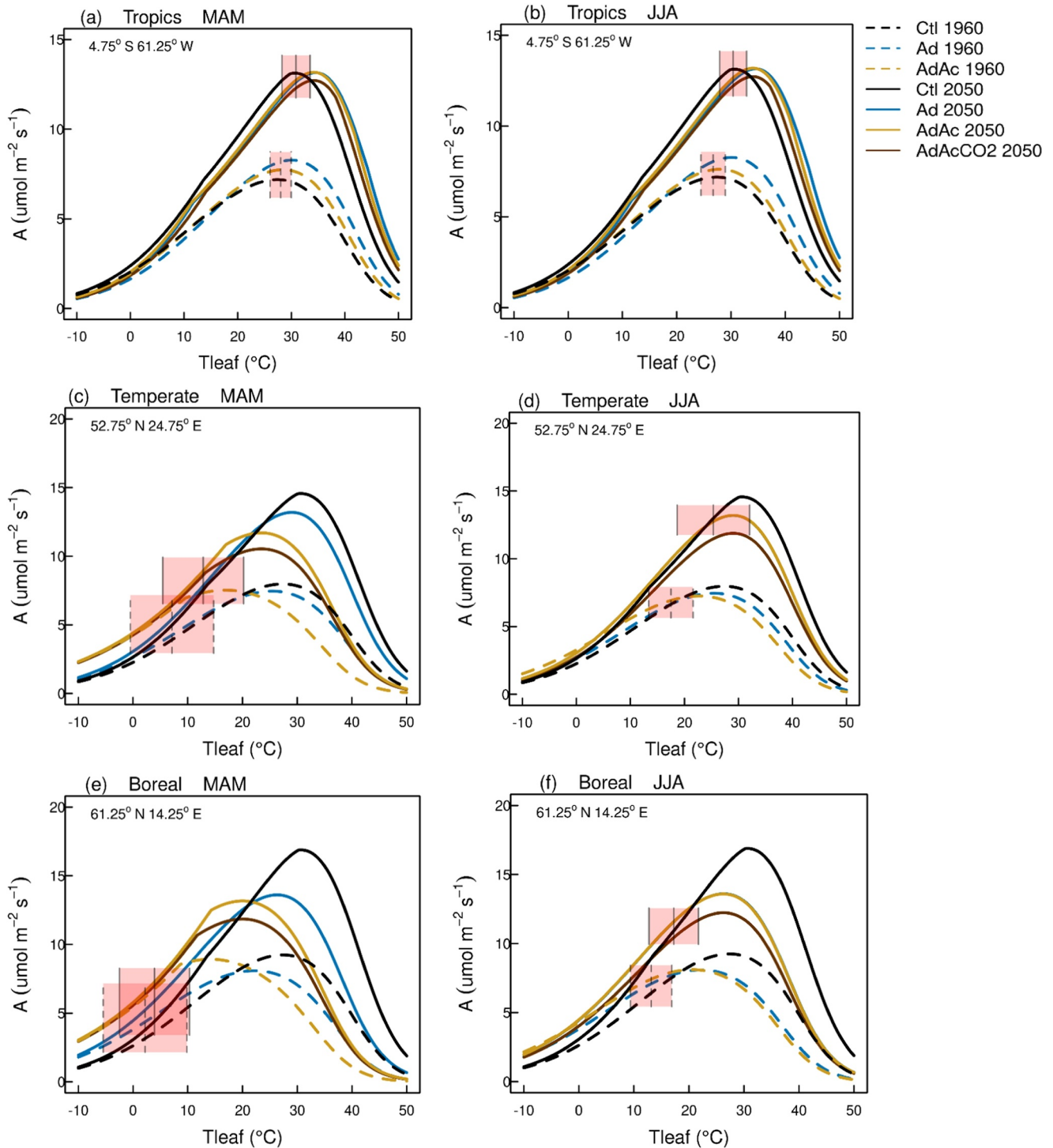


**Figure 3.** Leaf-level temperature response of light-saturated gross photosynthesis ( $A$ ) for sunlit leaves under *Ctl* (brown), *Ad* (blue), *AdAc* (yellow) and *AdAcCO2* (purple) in 1960 (dashed lines) and 2050 (solid lines) in (a, b) the tropical region ( $4.75^{\circ}\text{S}$ ,  $61.25^{\circ}\text{W}$ ) in MAM and JJA using PFT parameters for broadleaf evergreen tropical tree; (c,d) the temperate region ( $52.75^{\circ}\text{N}$ ,  $24.75^{\circ}\text{E}$ ) in MAM and JJA using PFT parameters for  $\text{C}_3$  grass; and (e,f) the boreal region ( $61.25^{\circ}\text{N}$ ,  $14.25^{\circ}\text{E}$ ) in MAM and JJA using PFT parameters for needleleaf evergreen tree. Shaded red areas represent the mean  $\pm 1$  SD daytime leaf temperature ( $T_{\text{leaf}}$ ) in 1960 (dashed gray lines), and 2050 (solid gray lines). Values used for mean  $T_{\text{leaf}}$ ,  $T_{\text{growth}}$  and  $T_{\text{home}}$  are shown in Table S4 in Supporting Information S1. Photosynthetically active radiation (PAR) is  $1,500 \mu\text{mol m}^{-2} \text{s}^{-1}$  in the tropics and  $1,000 \mu\text{mol m}^{-2} \text{s}^{-1}$  elsewhere. The atmospheric  $\text{CO}_2$  concentration is 315 ppm in 1960 and 566 ppm in 2050.

temperate region  $dGPP$  is  $1.1 \text{ PgC yr}^{-1}$  (16.2%) lower, and in the boreal region  $dGPP$  is  $0.2 \text{ PgC yr}^{-1}$  (7.7%) lower in  $AdAcCO_2$  than in  $Ctl$  (Table 3, Figure 2f).

### 3.3. Leaf-Level Analysis

The response of light-saturated gross photosynthesis ( $A$ ) to leaf temperature ( $T_{leaf}$ ) is shown in Figure 3 for three grid cells representing tropical, temperate and boreal regions. We use these leaf-level plots to understand the response of photosynthesis to adaptation and acclimation to temperature and  $CO_2$ . In all cases, the  $CO_2$  fertilization effect on photosynthesis increases  $A$  in 2050 compared to 1960, and  $T_{optA}$  also increases in response to elevated  $CO_2$ .

For the tropical broadleaf evergreen tree in 1960,  $T_{optV}$ ,  $T_{optJ}$ , and  $T_{optA}$  are highest with  $Ad$  (Figures 3a and 3b; Table S4 in Supporting Information S1). Under  $AdAc$ , adjustment of parameters to  $T_{growth}$  leads to lower values compared to  $Ad$ ; hence, over the range of simulated daytime hourly  $T_{leaf}$  in 1960, photosynthetic C uptake is greatest under  $Ad$ , followed by  $AdAc$ , and is lowest in  $Ctl$ . At the mean  $T_{leaf}$  in 1960, the rate of  $A$  in  $Ctl$  is at (in MAM) or very close to (in JJA)  $T_{optA}$ . Note that in 1960, no effect of  $AdAcCO_2$  was seen as atmospheric  $CO_2$  concentrations remained below the level at which acclimation of  $V_{cmax}$  and  $J_{max}$  to  $CO_2$  concentration occurred in our parameterization. In 2050, the simulated mean  $T_{leaf}$  has increased by  $\sim 3.0^\circ\text{C}$  which coincides closely with  $T_{optA}$  in  $Ctl$  ( $30.7^\circ\text{C}$ ) (Table S4 in Supporting Information S1). Above  $T_{optA}$ ,  $A$  simulated by  $Ctl$  therefore decreases with further increase in temperature. The range of leaf temperatures in 2050 from a minimum of  $25^\circ\text{C}$  to maximum of  $37^\circ\text{C}$  means that under  $Ctl$  photosynthetic C assimilation will frequently be negatively impacted by higher temperatures that are above  $T_{optA}$ .  $Ad$  has a higher  $T_{optV}$  and  $T_{optJ}$  compared to  $Ctl$  (note these parameters are unchanged between 1960 and 2050); however, the  $CO_2$  effect on  $T_{optA}$  increases it ( $34.5^\circ\text{C}$ ), so that  $T_{optA}$  sits well above the mean daytime  $T_{leaf}$  simulated in 2050 ( $30.9^\circ\text{C}$  in MAM) (Figures 3a and 3b). Under  $AdAc$ ,  $T_{optV}$  and  $T_{optJ}$  increase in 2050 compared with 1960 in response to increasing  $T_{growth}$ .  $V_{cmax}$  (increase) and  $J_{max}$  (decrease) at  $25^\circ\text{C}$  are also adjusted according to the change in local seasonal temperatures. At the mean daytime  $T_{leaf}$  simulated in 2050, photosynthesis is below  $T_{optA}$  (Figures 3a and 3b), so with increases in leaf temperature above the mean,  $A$  continues to increase. Therefore, under both  $Ad$  and  $AdAc$ , over the range of simulated daytime hourly  $T_{leaf}$  in 2050, photosynthetic carbon assimilation benefits from both adaptation and acclimation to temperature at higher  $T_{leaf}$  compared to  $Ctl$ . In 2050, the simulated response of  $Ad$  and  $AdAc$  are very similar because at this point  $T_{growth}$  is close to  $T_{home}$  (Table S4 in Supporting Information S1), but it is important to note that whereas  $T_{optV}$  and  $T_{optJ}$  are temporally fixed in  $Ad$ ,  $AdAc$  allows for temporal variation in  $T_{optV}$  and  $T_{optJ}$  allowing for further adjustment of these parameters as temperatures continue to rise beyond 2050. Under  $AdAcCO_2$  in 2050, although  $T_{optV}$  and  $T_{optJ}$  are not affected (Table S4 in Supporting Information S1),  $V_{cmax}$  and  $J_{max}$  at  $25^\circ\text{C}$  are down-regulated with the change being larger in  $V_{cmax}$ , leading to lower rates of  $CO_2$  assimilation at all  $T_{leaf}$ .

The temperate  $C_3$  grass and boreal needleleaf evergreen tree behaved similarly to each other (Figures 3c–3f). In both 1960 and 2050,  $T_{optV}$  and  $T_{optJ}$  are lower in  $Ad$  than in  $Ctl$ ,  $V_{cmax25}$  is lower and  $J_{max25}$  is higher in  $Ad$  than in  $Ctl$  (Table S4 in Supporting Information S1), which results in lower  $T_{optA}$  and C assimilation around  $T_{optA}$ . However, the range of simulated daytime hourly  $T_{leaf}$  in 1960 and 2050 in both these regions are not close to  $T_{optA}$ , and therefore over the cooler range of temperatures at which the leaf is operating, this results in higher rates of  $A$  under  $Ad$  compared to  $Ctl$  in both MAM and JJA (with the exception of  $C_3$  temperate grass in JJA above the mean daytime  $T_{leaf}$ ). Under  $AdAc$ ,  $T_{optV}$  and  $T_{optJ}$  are lower (more so in MAM than JJA) compared to both  $Ad$  and  $Ctl$  (Table S4 in Supporting Information S1), because of adjustment of these parameters to cooler seasonal  $T_{growth}$ . This leads to a lower  $T_{optA}$  but higher photosynthetic rate under  $AdAc$  over the mean daytime temperatures at which the leaf is operating, certainly in MAM (Figures 3c and 3e), in both 1960 and 2050. Acclimation to temperature therefore allows for adjustment of  $T_{optA}$  to the ambient seasonal temperature, which, although it results in a lower  $T_{optA}$ , allows plants to benefit from increased photosynthetic rates at lower  $T_{leaf}$ . The effect of acclimation to  $CO_2$  results in decreased  $A$  in 2050.  $T_{optV}$  and  $T_{optJ}$  are the same as  $AdAc$ , but in 2050  $V_{cmax25}$  and  $J_{max25}$  are lower under  $AdAcCO_2$  compared to  $AdAc$  (Table S4 in Supporting Information S1) resulting in reduced photosynthetic capacity.

## 4. Discussion

This study quantifies the individual and combined effects of adaptation and acclimation to temperature and acclimation to  $CO_2$  on projections of GPP under climate change. Incorporating these processes into JULES had a

net positive effect on simulated global GPP that persisted until 2050, despite weakening the rate of global C uptake by 13.5% over the simulation period relative to the control simulation without these processes. Temperature acclimation in temperate and boreal regions was the main driver of enhanced global GPP through adjustment of the photosynthetic temperature optimum to seasonal temperatures, which allowed higher rates of C assimilation. In the tropics, where photosynthesis is already operating near thermal optima, temperature acclimation increased  $T_{optA}$ , allowing higher photosynthetic rates to be maintained at elevated temperatures compared to the baseline simulation. However, temperature adaptation in warm tropical and subtropical regions drove the global decline in the rate of GPP enhancement over time. This was due to temperature-induced changes in the  $J_{max25}:V_{cmax25}$  ratio, which lowered the  $CO_2$  sensitivity of photosynthesis and weakened the  $CO_2$  fertilization response. These results therefore indicate that while temperature acclimation and adaptation of photosynthetic capacity improve thermal resilience of global GPP, these processes alter the temporal dynamics of global C uptake under climate change.  $CO_2$  acclimation of photosynthetic capacity down-regulates both biochemical parameters ( $V_{cmax25}$  and  $J_{max25}$ ), resulting in a consistent decline in the rate of GPP enhancement across biomes, although this response is more uncertain.

Comparison across modeling studies remains challenging given different interpretations and implementations of temperature acclimation algorithms, in particular acclimation of the  $J_{max25}:V_{cmax25}$  ratio (Mercado et al., 2018). In addition, the definition of the baseline simulation determines the effect size and direction, and this differs substantially between studies. Nevertheless, all studies agree that more physiologically realistic representations of the temperature sensitivity of photosynthetic capacity lead to enhanced absolute C uptake (Bennett et al., 2024; Knauer et al., 2023; Lombardozzi et al., 2015; Mercado et al., 2018; Oliver et al., 2022; Smith et al., 2016). Regional effects, however, remain inconsistent. In this study, temperature acclimation alone increased the rate of tropical C uptake over the simulation period, in agreement with Mercado et al. (2018) and Oliver et al. (2022), but in contrast with Smith et al. (2016) and Lombardozzi et al. (2015), who reported decreased vegetation C in the tropics. These latter studies used the Kattge and Knorr (2007) formulation, which does not explicitly separate acclimation from adaptation, and have differing approaches to acclimation of the  $J_{max25}:V_{cmax25}$  ratio. A more direct comparison can be made with Knauer et al. (2023), who, like this study, use the Kumarathunge et al. (2019) scheme, thereby explicitly accounting for both temperature adaptation and acclimation, albeit with a different implementation of  $J_{max25}:V_{cmax25}$  ratio acclimation. Comparison of our *AdAc* simulation to their “acclim” simulation—where acclimation of the  $J_{max25}:V_{cmax25}$  ratio is applied to  $J_{max}$  only—shows near neutral effects of temperature adaptation and acclimation on the GPP rate of change in the inner tropics, but a strong positive effect in the sub-tropics. In contrast, our *AdAc* simulation shows a weakened rate of GPP uptake, particularly in the inner tropics. Both studies, however, agreed on a reduced rate of GPP increase in temperate regions. Additionally, like this study, Knauer et al. (2023) found that changes in GPP trends are explained by the decreasing  $CO_2$  sensitivity of photosynthesis as photosynthesis becomes increasingly limited by  $J_{max}$  in warmer regions.

A key source of disagreement between modeling studies arises from how acclimation of the  $J_{max25}:V_{cmax25}$  ratio is implemented. Some studies (Smith et al. (2016), Lombardozzi et al. (2015), and Knauer et al. (2023) (in their “acclim” simulation)) reduce  $J_{max25}$  alone, while others (Mercado et al. (2018), Oliver et al. (2022), and this study) apply acclimation to both parameters while maintaining a constant leaf N concentration, such that decreasing  $J_{max25}$  increases  $V_{cmax25}$ . This approach assumes that plants optimally distribute available leaf N between  $V_{cmax}$  and  $J_{max}$ , and is implemented using a fixed ratio of N allocation based on observed relationships (Lin et al., 2013). This approach is taken because whilst many studies report a decline in the  $J_{max25}:V_{cmax25}$  ratio with increasing  $T_{growth}$  (Crous et al., 2022; Dusenge et al., 2020; Kattge & Knorr, 2007; Kumarathunge et al., 2019), it is less clear whether this arises from a change in  $V_{cmax25}$ ,  $J_{max25}$  or both (Choury et al., 2022; Kumarathunge et al., 2019; Lamba et al., 2018; Scafaro et al., 2017; Smith & Dukes, 2017).

These differing assumptions regarding the  $J_{max25}:V_{cmax25}$  ratio likely explain the lower tropical GPP in the studies of Smith et al. (2016) and Lombardozzi et al. (2015), where only  $J_{max25}$  declines. Knauer et al. (2023), for example, have an alternative implementation of the  $J_{max25}:V_{cmax25}$  ratio, which is independent of temperature and adjusts the  $J_{max25}:V_{cmax25}$  ratio dynamically according to leaf N availability to maximize net canopy photosynthesis. This is an optimization approach based on the “coordination hypothesis” that assumes that leaf N is redistributed between the  $CO_2$ - and light-limited processes of C assimilation, and leads to approximately equal contribution of the two limiting rates to canopy photosynthesis. The limitation imposed on photosynthesis by a low  $J_{max25}$  (as seen in their “acclim” simulation) is removed and a higher tropical GPP is maintained. Comparison of these two implementations within a single study demonstrates the sensitivity of GPP projections to how

acclimation of the  $J_{max25}:V_{cmax25}$  ratio is represented, underlining the need for further empirical data to understand how much of the change in this ratio with warming is due to  $V_{cmax25}$  versus  $J_{max25}$ .

Focusing on the response of photosynthetic capacity to temperature adaptation and acclimation alone, our results show that the large slowdown in the rate of global GPP enhancement is due to the effect of temperature adaptation on the  $J_{max25}:V_{cmax25}$  ratio in tropical and subtropical regions with a high  $T_{home}$ . Our temperature adaptation alone (*Ad*) simulation causes a larger decrease in the  $J_{max25}:V_{cmax25}$  ratio compared to either our baseline (*Ctl*) or *AdAc* simulation. Greater limitation of photosynthesis by  $J_{max25}$  reduced the CO<sub>2</sub> sensitivity of photosynthesis, leading to a weaker GPP response to rising CO<sub>2</sub>. This aligns with warming experiments on tropical tree seedlings that show photosynthesis to be increasingly limited by  $J_{max}$  as growth temperatures increase (Choury et al., 2022; Slot & Winter, 2017; Vårhammar et al., 2015). Physiologically, a reduction in  $J_{max}$  at high temperatures occurs to avoid thermal damage to the thylakoid membrane, because  $J_{max}$  has a greater dependence upon membrane stability (to maintain energy generation via the electron transport chain) compared to  $V_{cmax}$  (Hikosaka et al., 2005).

Our leaf-level simulations demonstrate that adjustment of  $T_{optV}$  and  $T_{optJ}$  to temperature, and the resulting change in  $T_{optA}$ , allows plants to benefit from higher rates of CO<sub>2</sub> assimilation at the mean daytime  $T_{leaf}$  experienced by the vegetation growing under 1960 conditions. As  $T_{growth}$  rises, acclimation of  $T_{optV}$  and  $T_{optJ}$  to temperature increases  $T_{optA}$ . In these simulations, photosynthesis in tropical trees is operating close to its thermal optimum in both 1960 and 2050. However, as temperatures rise in the future, tropical trees increase their  $T_{optA}$ , demonstrating increased thermal resilience. On days experiencing temperatures that are higher than the fixed  $T_{optA}$  of our *Ctl* simulation, photosynthesis is higher in acclimated trees compared to unacclimated *Ctl* trees, whose rate of photosynthesis declines with further increase in temperature. However, when  $T_{leaf}$  is below  $T_{optA}$ , photosynthesis in acclimating trees is often lower than *Ctl* trees. Reduced photosynthetic rates in tropical tree species at high  $T_{growth}$ , despite temperature acclimation, are not unusual and have been found in experimental studies (Choury et al., 2022; Crous et al., 2022; Dusenge et al., 2021; Slot & Winter, 2017). Choury et al. (2022) showed that tropical and subtropical rainforest species acclimate to increasing  $T_{growth}$  (increased  $T_{optA}$ ), but photosynthesis is reduced at higher temperatures, indicating that tropical species have increased thermal resilience to warming but may reduce C uptake at higher temperatures. In this study, photosynthesis of the temperate C<sub>3</sub> grasses and boreal needleleaf evergreen trees is operating well below its thermal optimum, and C assimilation benefits from thermal acclimation by adjustment of  $T_{optA}$  to the lower  $T_{growth}$  characteristic of these regions. The implementation of photosynthetic capacity temperature acclimation in our study therefore lowers the risk of thermal stress on modeled C uptake as global temperatures rise, particularly in tropical regions where trees are operating close to their  $T_{optA}$ .

In contrast, acclimation of photosynthetic capacity to eCO<sub>2</sub> causes a widespread decline in the rate of C uptake over the simulation period, though with substantial uncertainty—especially in the tropics where a big data gap exists. Most evidence for CO<sub>2</sub> responses comes from first generation free-air CO<sub>2</sub> enrichment (FACE) studies which, for forests, are usually young trees in their exponential growth phase. These forest FACE experiments report large enhancements of photosynthesis in eCO<sub>2</sub> (30%–60%) depending on species and environmental conditions (Ainsworth & Long, 2005; Ainsworth & Rogers, 2007). Whilst many studies report photosynthetic downregulation (Ainsworth & Rogers, 2007; Crous & Ellsworth, 2004; Leakey et al., 2009), others find no such response (Crous et al., 2008; Herrick & Thomas, 2001; Warren et al., 2015). Second-generation FACE experiments with mature trees suggest more variable responses. For example, there was no evidence of photosynthetic downregulation to eCO<sub>2</sub> in a 100-year-old mature deciduous forest (Bader et al., 2010), no photosynthetic downregulation was observed in a 175-year-old deciduous woodland (Gardner et al., 2021), and photosynthetic downregulation of  $V_{cmax}$  only was observed in a 70-year old Eucalypt woodland (Yang et al., 2020). However, these studies span short timescales, which may not be long enough for downregulation to occur. Recent data from the central Amazon rainforest showed no downregulation of photosynthetic capacity in response to eCO<sub>2</sub> in understory plants (Damasceno et al., 2024). The  $J_{max}:V_{cmax}$  ratio increased as a result of an increase in  $J_{max}$  and no change in  $V_{cmax}$  (Damasceno et al., 2024). However, the relatively short observation period may not have given sufficient time for downregulation to occur in these shade plants, and the results may not translate to mature top-of-canopy trees. Therefore, more data is urgently needed to understand and quantify the nature of acclimation of photosynthetic capacity to CO<sub>2</sub>, especially in tropical forests where there is a notable knowledge gap.

Several mechanisms could explain photosynthetic CO<sub>2</sub> acclimation. Nutrient limitation is one of the primary explanations: if soil nutrient supply is insufficient to match increased C uptake, foliar nutrient concentrations

may fall, leading to a reduction in photosynthetic capacity. Alternatively, source-sink imbalances—where carbohydrate production in leaves (the source, which is upregulated in response to elevated CO<sub>2</sub>) exceeds the demand for carbohydrates in growing tissues (the sink)—may lead to photosynthetic downregulation to avoid excessive carbohydrate accumulation (Ainsworth & Rogers, 2007; Ainsworth et al., 2004). Another hypothesis is that plants adjust photosynthetic capacity to optimize resource use, maintaining high C fixation rates with minimal resource investment (Maschler et al., 2022; Smith & Keenan, 2020). Under eCO<sub>2</sub>, enhanced leaf-level photosynthesis reduces leaf nutrient demand, allowing plants to reallocate nutrients to either invest in photosynthetic machinery or other growth processes such as increased leaf area or root development. This response could alleviate potential nutrient limitations that may constrain the response to CO<sub>2</sub> (Smith et al., 2024; Smith & Keenan, 2020). Our model of CO<sub>2</sub> acclimation, which reduces  $V_{cmax}$  more than  $J_{max}$ , reflects reallocation within the leaf, but does not simulate broader growth reallocations such as increased leaf area or root development. Including such processes in our model could mitigate the large GPP decline with CO<sub>2</sub> acclimation, particularly in nitrogen-limited regions; however, parameterizing dynamic nutrient allocation in global vegetation models remains a significant challenge.

Nutrient limitations—especially nitrogen and phosphorus—add uncertainty to our simulations. While limited nitrogen availability and the immobilization of nitrogen (progressive nitrogen limitation) have long been recognized as constraints on plant photosynthetic and growth responses to eCO<sub>2</sub> (Ainsworth & Long, 2005; Terrer et al., 2019; Wang & Wang, 2021), phosphorus limitation is increasingly seen as critical, particularly in tropical ecosystems (Cunha et al., 2022; Du et al., 2020; Ellsworth et al., 2017; Jiang, Caldararu, et al., 2020; Jiang, Medlyn, et al., 2020). Our simulations do not include nitrogen or phosphorus cycling. This assumption of unlimited nutrient supply may mean that our simulations overestimate GPP in tropical ecosystems that are dominantly phosphorus limited (Cunha et al., 2022; Fleischer et al., 2019), and overestimate GPP in temperate ecosystems that tend to be more nitrogen-limited. This highlights the need for improved representations of nutrient constraints in Earth System models and potential feedbacks between nutrient availability and other processes such as CO<sub>2</sub> acclimation.

An additional limitation arises from the use of a prescribed seasonally varying annual climatology of *LAI* (i.e., no response to changes in CO<sub>2</sub> or interannual variability) in our simulations. Dynamic *LAI* responses to eCO<sub>2</sub> can affect leaf temperature and water balance through several competing mechanisms (De Kauwe et al., 2014). Given that leaf temperature is a primary driver of photosynthetic rate, *LAI*-mediated feedbacks could impact simulated GPP. For example, while a larger canopy allows greater interception and transpiration potentially leading to lower leaf temperatures through increased evaporative cooling, reduced stomatal conductance under eCO<sub>2</sub> may increase leaf temperatures (Ainsworth & Rogers, 2007). Canopy structure also affects radiation absorption and shading. A denser canopy absorbs more solar radiation, potentially raising sunlit and top of the canopy leaf temperatures, although self-shading within the canopy can mitigate this effect. The JULES model diagnoses a surface canopy temperature and this is used to drive the photosynthesis model; however, our use of “fixed” *LAI* fails to fully capture these *LAI*-mediated feedbacks on leaf energy balance and temperature that could potentially influence our results. The precise impact of dynamic *LAI* on the simulated GPP in this study remains challenging to predict due to the complex interplay of competing feedbacks, but would be important to explore in future work.

Finally, a major knowledge gap is the lack of algorithms for temperature adaptation and acclimation of photosynthetic capacity in C<sub>4</sub> plants. Many tropical grasses and important agricultural crops use the C<sub>4</sub> photosynthetic pathway, but existing acclimation schemes, including the one used in this study, are developed only for C<sub>3</sub> vegetation. Acclimation of photosynthetic capacity to temperature has been demonstrated for C<sub>4</sub> plants (Yamori et al., 2014); however, fewer empirical studies exist for C<sub>4</sub> vegetation compared to C<sub>3</sub>. As a result, no robust algorithms are currently available for implementation of C<sub>4</sub> temperature acclimation into LSMs, although recent developments have been made using optimality theory (Scott & Smith, 2022).

## 5. Conclusion

To conclude, our results suggest that allowing photosynthetic capacity to adjust to local growth temperatures enhances the thermal resilience of GPP to rising temperatures, particularly in tropical forests operating near their temperature optimum. Our results show that dynamically adjusting the  $J_{max25} : V_{cmax25}$  ratio in response to temperature alters the CO<sub>2</sub> sensitivity of photosynthesis. In these simulations, the CO<sub>2</sub> fertilization response of photosynthesis was weakened in warm tropical regions. Accounting for temperature adaptation and acclimation

therefore affects both the magnitude and temporal dynamics of C uptake by terrestrial ecosystems, which could impact land-atmosphere feedbacks, and have potential implications for future climate projections. Our results further highlight a strong sensitivity of GPP to the downregulation of photosynthetic capacity under eCO<sub>2</sub>; however, this response is more uncertain. Altogether, our results suggest that models that do not consider the additional physiological realism of these processes that determine photosynthetic capacity may underestimate global C uptake, and may fail to capture important spatial variability of land C uptake and storage under future conditions. Finally, this study emphasizes the need for more targeted data to disentangle the components driving temperature acclimation of the  $J_{max25}:V_{cmax25}$  ratio, and to better quantify photosynthetic acclimation to CO<sub>2</sub>, especially in tropical forests.

## Data Availability Statement

JULES-vn5.6 was used for all simulations. The JULES model code and suites used to run the model are available from the Met Office Science Repository Service (MOSRS). Registration is required and the code is freely available to anyone for non-commercial use. To access the repository, complete the online form here: [http://jules-lsm.github.io/access\\_req/JULES\\_access.html](http://jules-lsm.github.io/access_req/JULES_access.html). The results presented in this paper were obtained by running JULES from the following branch: <https://code.metoffice.gov.uk/trac/jules/browser/main/branches/dev/douglasclark>. This is a development branch of JULES-vn5.6 to include acclimation of photosynthetic capacity to temperature and CO<sub>2</sub>, as described in this paper. This branch can be accessed and downloaded from the Met Office Science Repository Service once the user has registered for an account, as outlined above. Documentation for the JULES model is located here: <https://jules-lsm.github.io/vn5.6/>. Site-level simulations used the rose suite u-br064 (<https://code.metoffice.gov.uk/trac/roses-u/browser/br/0/6/4/> at revision 146216), which is a copy of the u-al752 JULES suite for FLUXNET 2015 and LBA sites described here <https://code.metoffice.gov.uk/trac/jules/wiki/FluxnetandLbaSites>, and downloaded from here <https://code.metoffice.gov.uk/trac/roses-u/browser/a/1/7/5/2/> see Harper et al. (2021). The global simulations used the JULES rose suite u-bq898 (McGuire et al., 2022), which uses the Global Land configuration 7.1 (Wiltshire et al., 2020). Suites can be downloaded from MOSRS once the user has registered for an account.

## Acknowledgments

Authors thank Pier Luigi Vidale, Patrick McGuire and Markus Todt (Department of Meteorology and National Centre for Atmospheric Science, Reading University) for their support with the model forcing data and the JULES suite (u-bq898). The authors also thank the developers of the JULES suite for FLUXNET 2015 and LBA sites (u-al752). R.J.O., L.M.M and P.P.H acknowledge funding from the UK Natural Environment Research Council (NERC) for the TerraFIRMA project (NE/W004895/1). This work was also supported by NERC as part of the NC for Global Challenges programme (NE/X006247/1) delivering National Capability. L.M.M acknowledges the NERC projects NE/R001928/1 and NE/X001172/1. B.E.M is supported by an Australian Research Council Laureate Fellowship FL190100003. This work used eddy covariance data acquired and shared by the FLUXNET community, including these networks: AmeriFlux, AfriFlux, AsiaFlux, CarboAfrica, CarboEuropeIP, CarboItaly, CarboMont, ChinaFlux, Fluxnet-Canada, GreenGrass, ICOS, KoFlux, LBA, NECC, OzFlux-TERN, TCOS-Siberia and USCCC. The ERA-Interim reanalysis data were provided by ECMWF and processed by LSCE. The FLUXNET eddy covariance data processing and harmonization was carried out by the European Fluxes Database Cluster, AmeriFlux Management Project, and Fluxdata project of FLUXNET, with the support of CDIAC and ICOS Ecosystem Thematic Center, and the OzFlux, ChinaFlux and AsiaFlux offices.

## References

- Ainsworth, E. A., & Long, S. P. (2005). What have we learned from 15 years of free-air CO<sub>2</sub> enrichment (FACE)? A meta-analytic review of the responses of photosynthesis, canopy properties and plant production to rising CO<sub>2</sub>. *New Phytologist*, *165*(2), 351–372. <https://doi.org/10.1111/j.1469-8137.2004.01224.x>
- Ainsworth, E. A., & Rogers, A. (2007). The response of photosynthesis and stomatal conductance to rising [CO<sub>2</sub>]: Mechanisms and environmental interactions. *Plant, Cell and Environment*, *30*(3), 258–270. <https://doi.org/10.1111/j.1365-3040.2007.01641.x>
- Ainsworth, E. A., Rogers, A., Nelson, R., & Long, S. P. (2004). Testing the “source–sink” hypothesis of down-regulation of photosynthesis in elevated [CO<sub>2</sub>] in the field with single gene substitutions in Glycine max. *Agricultural and Forest Meteorology*, *122*(1), 85–94. <https://doi.org/10.1016/j.agrformet.2003.09.002>
- Arora, V. K., Katavouta, A., Williams, R. G., Jones, C. D., Brovkin, V., Friedlingstein, P., et al. (2020). Carbon–concentration and carbon–climate feedbacks in CMIP6 models and their comparison to CMIP5 models. *Die BG*, *17*(16), 4173–4222. <https://doi.org/10.5194/bg-17-4173-2020>
- Bader, M. K.-F., Siegwolf, R., & Körner, C. (2010). Sustained enhancement of photosynthesis in mature deciduous forest trees after 8 years of free air CO<sub>2</sub> enrichment. *Planta*, *232*(5), 1115–1125. <https://doi.org/10.1007/s00425-010-1240-8>
- Bennett, A. C., Knauer, J., Bennett, L. T., Haverd, V., & Arndt, S. K. (2024). Variable influence of photosynthetic thermal acclimation on future carbon uptake in Australian wooded ecosystems under climate change. *Global Change Biology*, *30*(1), e17021. <https://doi.org/10.1111/gcb.17021>
- Benomar, L., Lamhamedi, M. S., Pepin, S., Rainville, A., Lambert, M.-C., Margolis, H. A., et al. (2017). Thermal acclimation of photosynthesis and respiration of southern and northern white spruce seed sources tested along a regional climatic gradient indicates limited potential to cope with temperature warming. *Annals of Botany*, *121*(3), 443–457. <https://doi.org/10.1093/aob/mcx174>
- Bernacchi, C. J., Singaas, E. L., Pimentel, C., Portis Jr, A. R., & Long, S. P. (2001). Improved temperature response functions for models of Rubisco-limited photosynthesis. *Plant, Cell and Environment*, *24*(2), 253–259. <https://doi.org/10.1111/j.1365-3040.2001.00668.x>
- Berry, J. A., & Bjorkman, O. (1980). Photosynthetic response and adaptation to temperature in higher plants. *Annual Review of Plant Physiology*, *31*(1), 491–543. <https://doi.org/10.1146/annurev.pp.31.060180.002423>
- Best, M. J., Pryor, M., Clark, D. B., Rooney, G. G., Essery, R. L. H., Ménard, C. B., et al. (2011). The joint UK land environment simulator (JULES), model description – Part 1: Energy and water fluxes. *Geoscientific Model Development*, *4*(3), 677–699. <https://doi.org/10.5194/gmd-4-677-2011>
- Booth, B. B. B., Jones, C. D., Collins, M., Totterdell, I. J., Cox, P. M., Sitch, S., et al. (2012). High sensitivity of future global warming to land carbon cycle processes. *Environmental Research Letters*, *7*(2), 024002. <https://doi.org/10.1088/1748-9326/7/2/024002>
- Carter, K. R., Wood, T. E., Reed, S. C., Schwartz, E. C., Reinsel, M. B., Yang, X., & Cavaleri, M. A. (2020). Photosynthetic and respiratory acclimation of understory shrubs in response to in situ experimental warming of a wet tropical forest. *Frontiers in Forests and Global Change*, *3*(114). <https://doi.org/10.3389/ffgc.2020.576320>
- Choury, Z., Wujeska-Klaus, A., Bourne, A., Bown, N. P., Tjoelker, M. G., Medlyn, B. E., & Crous, K. Y. (2022). Tropical rainforest species have larger increases in temperature optima with warming than warm-temperate rainforest trees. *New Phytologist*, *234*(4), 1220–1236. <https://doi.org/10.1111/nph.18077>

- Clark, D. B., Mercado, L. M., Sitch, S., Jones, C. D., Gedney, N., Best, M. J., et al. (2011). The Joint UK Land Environment Simulator (JULES), model description – Part 2: Carbon fluxes and vegetation dynamics. *Geoscientific Model Development*, 4(3), 701–722. <https://doi.org/10.5194/gmd-4-701-2011>
- Collatz, G. J., Ball, J. T., Grivet, C., & Berry, J. A. (1991). Physiological and environmental regulation of stomatal conductance, photosynthesis and transpiration: A model that includes a laminar boundary layer. *Agricultural and Forest Meteorology*, 54(2), 107–136. [https://doi.org/10.1016/0168-1923\(91\)90002-8](https://doi.org/10.1016/0168-1923(91)90002-8)
- Cox, A. J. F., Hartley, I. P., Meir, P., Sitch, S., Dusenage, M. E., Restrepo, Z., et al. (2023). Acclimation of photosynthetic capacity and foliar respiration in Andean tree species to temperature change. *New Phytologist*, 238(6), 2329–2344. <https://doi.org/10.1111/nph.18900>
- Crous, K. Y., & Ellsworth, D. S. (2004). Canopy position affects photosynthetic adjustments to long-term elevated CO<sub>2</sub> concentration (FACE) in aging needles in a mature Pinus taeda forest. *Tree Physiology*, 24(9), 961–970. <https://doi.org/10.1093/treephys/24.9.961>
- Crous, K. Y., Uddling, J., & De Kauwe, M. G. (2022). Temperature responses of photosynthesis and respiration in evergreen trees from boreal to tropical latitudes. *New Phytologist*, 234(2), 353–374. <https://doi.org/10.1111/nph.17951>
- Crous, K. Y., Walters, M. B., & Ellsworth, D. S. (2008). Elevated CO<sub>2</sub> concentration affects leaf photosynthesis–nitrogen relationships in Pinus taeda over nine years in FACE. *Tree Physiology*, 28(4), 607–614. <https://doi.org/10.1093/treephys/28.4.607>
- Cunha, H. F. V., Andersen, K. M., Lugli, L. F., Santana, F. D., Aleixo, I. F., Moraes, A. M., et al. (2022). Direct evidence for phosphorus limitation on Amazon forest productivity. *Nature*, 608(7923), 558–562. <https://doi.org/10.1038/s41586-022-05085-2>
- Damasceno, A. R., Garcia, S., Aleixo, I. F., Menezes, J. C. G., Pereira, I. S., De Kauwe, M. G., et al. (2024). In situ short-term responses of Amazonian understory plants to elevated CO<sub>2</sub>. *Plant, Cell and Environment*, 47(5), 1865–1876. <https://doi.org/10.1111/pce.14842>
- De Kauwe, M. G., Medlyn, B. E., Zaehle, S., Walker, A. P., Dietze, M. C., Wang, Y.-P., et al. (2014). Where does the carbon go? A model–data intercomparison of vegetation carbon allocation and turnover processes at two temperate forest free-air CO<sub>2</sub> enrichment sites. *New Phytologist*, 203(3), 883–899. <https://doi.org/10.1111/nph.12847>
- Domingues, T. F., Meir, P., Feldpausch, T. R., Saiz, G., Veenendaal, E. M., Schrod, F., et al. (2010). Co-limitation of photosynthetic capacity by nitrogen and phosphorus in West Africa woodlands. *Plant, Cell and Environment*, 33(6), 959–980. <https://doi.org/10.1111/j.1365-3040.2010.02119.x>
- Drake, J. E., Aspinwall, M. J., Pfautsch, S., Rymer, P. D., Reich, P. B., Smith, R. A., et al. (2015). The capacity to cope with climate warming declines from temperate to tropical latitudes in two widely distributed Eucalyptus species. *Global Change Biology*, 21(1), 459–472. <https://doi.org/10.1111/gcb.12729>
- Du, E., Terrer, C., Pellegrini, A. F. A., Ahlström, A., van Lissa, C. J., Zhao, X., et al. (2020). Global patterns of terrestrial nitrogen and phosphorus limitation. *Nature Geoscience*, 13(3), 221–226. <https://doi.org/10.1038/s41561-019-0530-4>
- Dusenage, M. E., Madhavji, S., & Way, D. A. (2020). Contrasting acclimation responses to elevated CO<sub>2</sub> and warming between an evergreen and a deciduous boreal conifer. *Global Change Biology*, 26(6), 3639–3657. <https://doi.org/10.1111/gcb.15084>
- Dusenage, M. E., Witemann, M., Mujawamariya, M., Ntawuhiganayo, E. B., Zibera, E., Ntirugulirwa, B., et al. (2021). Limited thermal acclimation of photosynthesis in tropical montane tree species. *Global Change Biology*, 27(19), 4860–4878. <https://doi.org/10.1111/gcb.15790>
- Ellsworth, D. S., Anderson, I. C., Crous, K. Y., Cooke, J., Drake, J. E., Gherlenda, A. N., et al. (2017). Elevated CO<sub>2</sub> does not increase eucalypt forest productivity on a low-phosphorus soil. *Nature Climate Change*, 7(4), 279–282. <https://doi.org/10.1038/nclimate3235>
- Evans, J. R., & Poorter, H. (2001). Photosynthetic acclimation of plants to growth irradiance: The relative importance of specific leaf area and nitrogen partitioning in maximizing carbon gain. *Plant, Cell and Environment*, 24(8), 755–767. <https://doi.org/10.1046/j.1365-3040.2001.00724.x>
- Farquhar, G. D., von Caemmerer, S., & Berry, J. A. (1980). A biochemical model of photosynthetic CO<sub>2</sub> assimilation in leaves of C<sub>3</sub> species. *Planta*, 149(1), 78–90. <https://doi.org/10.1007/BF00386231>
- Fleischer, K., Rammig, A., De Kauwe, M. G., Walker, A. P., Domingues, T. F., Fuchslueger, L., et al. (2019). Amazon forest response to CO<sub>2</sub> fertilization dependent on plant phosphorus acquisition. *Nature Geoscience*, 12(9), 736–741. <https://doi.org/10.1038/s41561-019-0404-9>
- Friedlingstein, P., Meinshausen, M., Arora, V. K., Jones, C. D., Anav, A., Liddicoat, S. K., & Knutti, R. (2014). Uncertainties in CMIP5 climate projections due to carbon cycle feedbacks. *Journal of Climate*, 27(2), 511–526. <https://doi.org/10.1175/JCLI-D-12-00579.1>
- Friedlingstein, P., O'Sullivan, M., Jones, M. W., Andrew, R. M., Gregor, L., Hauck, J., et al. (2022). Global carbon budget 2022. *Earth System Science Data*, 14(11), 4811–4900. <https://doi.org/10.5194/essd-14-4811-2022>
- Gardner, A., Ellsworth, D. S., Crous, K. Y., Pritchard, J., & MacKenzie, A. R. (2021). Is photosynthetic enhancement sustained through three years of elevated CO<sub>2</sub> exposure in 175-year-old Quercus robur? *Tree Physiology*, 42(1), 130–144. <https://doi.org/10.1093/treephys/tpab090>
- Guha, A., Han, J., Cummings, C., McLennan, D. A., & Warren, J. M. (2018). Differential ecophysiological responses and resilience to heat wave events in four co-occurring temperate tree species. *Environmental Research Letters*, 13(6), 065008. <https://doi.org/10.1088/1748-9326/aabcd8>
- Gunderson, C. A., O'Hara, K. H., Campion, C. M., Walker, A. V., & Edwards, N. T. (2010). Thermal plasticity of photosynthesis: The role of acclimation in forest responses to a warming climate. *Global Change Biology*, 16(8), 2272–2286. <https://doi.org/10.1111/j.1365-2486.2009.02090.x>
- Haarsma, R. J., Roberts, M. J., Vidale, P. L., Senior, C. A., Bellucci, A., Bao, Q., et al. (2016). High resolution model intercomparison project (HighResMIP v1.0) for CMIP6. *Geoscientific Model Development*, 9(11), 4185–4208. <https://doi.org/10.5194/gmd-9-4185-2016>
- Harper, A. B., Cox, P. M., Friedlingstein, P., Wiltshire, A. J., Jones, C. D., Sitch, S., et al. (2016). Improved representation of plant functional types and physiology in the Joint UK Land Environment Simulator (JULES v4.2) using plant trait information. *Geoscientific Model Development*, 9(7), 2415–2440. <https://doi.org/10.5194/gmd-9-2415-2016>
- Harper, A. B., Williams, K. E., McGuire, P. C., Duran Rojas, M. C., Hemming, D., Verhoef, A., et al. (2021). Improvement of modeling plant responses to low soil moisture in JULESv4.9 and evaluation against flux tower measurements. *Geoscientific Model Development*, 14(6), 3269–3294. <https://doi.org/10.5194/gmd-14-3269-2021>
- Haverd, V., Smith, B., Nieradzki, L., Briggs, P. R., Woodgate, W., Trudinger, C. M., et al. (2018). A new version of the CABLE land surface model (Subversion revision r4601) incorporating land use and land cover change, woody vegetation demography, and a novel optimisation-based approach to plant coordination of photosynthesis. *Geoscientific Model Development*, 11(7), 2995–3026. <https://doi.org/10.5194/gmd-11-2995-2018>
- Herrick, J., & Thomas, R. (2001). No photosynthetic down-regulation in sweetgum trees (*Liquidambar styraciflua* L.) after three years of CO<sub>2</sub> enrichment at the Duke Forest FACE experiment. *Plant, Cell and Environment*, 24(1), 53–64. <https://doi.org/10.1046/j.1365-3040.2001.00652.x>
- Hikosaka, K., Ishikawa, K., Borjigidai, A., Muller, O., & Onoda, Y. (2005). Temperature acclimation of photosynthesis: Mechanisms involved in the changes in temperature dependence of photosynthetic rate. *Journal of Experimental Botany*, 57(2), 291–302. <https://doi.org/10.1093/jxb/erj049>

- Hikosaka, K., Nabeshima, E., & Hiura, T. (2007). Seasonal changes in the temperature response of photosynthesis in canopy leaves of *Quercus crispula* in a cool-temperate forest. *Tree Physiology*, 27(7), 1035–1041. <https://doi.org/10.1093/treephys/27.7.1035>
- Jiang, M., Caldararu, S., Zhang, H., Fleischer, K., Crous, K. Y., Yang, J., et al. (2020). Low phosphorus supply constrains plant responses to elevated CO<sub>2</sub>: A meta-analysis. *Global Change Biology*, 26(10), 5856–5873. <https://doi.org/10.1111/gcb.15277>
- Jiang, M., Medlyn, B. E., Drake, J. E., Duursma, R. A., Anderson, I. C., Barton, C. V. M., et al. (2020). The fate of carbon in a mature forest under carbon dioxide enrichment. *Nature*, 580(7802), 227–231. <https://doi.org/10.1038/s41586-020-2128-9>
- Kattge, J., & Knorr, W. (2007). Temperature acclimation in a biochemical model of photosynthesis: A reanalysis of data from 36 species. *Plant, Cell and Environment*, 30(9), 1176–1190. <https://doi.org/10.1111/j.1365-3040.2007.01690.x>
- Knauer, J., Cuntz, M., Smith, B., Canadell, J. G., Medlyn, B. E., Bennett, A. C., et al. (2023). Higher global gross primary productivity under future climate with more advanced representations of photosynthesis. *Science Advances*, 9(46), eadh9444. <https://doi.org/10.1126/sciadv.adh9444>
- Kroner, Y., & Way, D. A. (2016). Carbon fluxes acclimate more strongly to elevated growth temperatures than to elevated CO<sub>2</sub> concentrations in a northern conifer. *Global Change Biology*, 22(8), 2913–2928. <https://doi.org/10.1111/gcb.13215>
- Kumarathunge, D. P., Medlyn, B. E., Drake, J. E., Tjoelker, M. G., Aspinwall, M. J., Battaglia, M., et al. (2019). Acclimation and adaptation components of the temperature dependence of plant photosynthesis at the global scale. *New Phytologist*, 222(2), 768–784. <https://doi.org/10.1111/nph.15668>
- Kurepin, L. V., Stangl, Z. R., Ivanov, A. G., Bui, V., Mema, M., Hüner, N. P. A., et al. (2018). Contrasting acclimation abilities of two dominant boreal conifers to elevated CO<sub>2</sub> and temperature. *Plant, Cell and Environment*, 41(6), 1331–1345. <https://doi.org/10.1111/pce.13158>
- Lamba, S., Hall, M., Råntfors, M., Chaudhary, N., Linder, S., Way, D., et al. (2018). Physiological acclimation dampens initial effects of elevated temperature and atmospheric CO<sub>2</sub> concentration in mature boreal Norway spruce. *Plant, Cell and Environment*, 41(2), 300–313. <https://doi.org/10.1111/pce.13079>
- Lawrence, D. M., Fisher, R. A., Koven, C. D., Oleson, K. W., Swenson, S. C., Bonan, G., et al. (2019). The community land model version 5: Description of new features, benchmarking, and impact of forcing uncertainty. *Journal of Advances in Modeling Earth Systems*, 11(12), 4245–4287. <https://doi.org/10.1029/2018MS001583>
- Leakey, A. D. B., Ainsworth, E. A., Bernacchi, C. J., Rogers, A., Long, S. P., & Ort, D. R. (2009). Elevated CO<sub>2</sub> effects on plant carbon, nitrogen, and water relations: Six important lessons from FACE. *Journal of Experimental Botany*, 60(10), 2859–2876. <https://doi.org/10.1093/jxb/erp096>
- Lin, Y.-S., Medlyn, B. E., De Kauwe, M. G., & Ellsworth, D. S. (2013). Biochemical photosynthetic responses to temperature: How do interspecific differences compare with seasonal shifts? *Tree Physiology*, 33(8), 793–806. <https://doi.org/10.1093/treephys/tpu047>
- Lombardozzi, D. L., Bonan, G. B., Smith, N. G., Dukes, J. S., & Fisher, R. A. (2015). Temperature acclimation of photosynthesis and respiration: A key uncertainty in the carbon cycle-climate feedback. *Geophysical Research Letters*, 42(20), 8624–8631. <https://doi.org/10.1002/2015GL065934>
- Maschler, J., Bialic-Murphy, L., Wan, J., Andresen, L. C., Zohner, C. M., Reich, P. B., et al. (2022). Links across ecological scales: Plant biomass responses to elevated CO<sub>2</sub>. *Global Change Biology*, 28(21), 6115–6134. <https://doi.org/10.1111/gcb.16351>
- McGuire, P. C., Vidale, P. L., Lister, G. M. S., Martinez de la Torre, A., Muller, O. V., & Todt, M. (2022). Rose suite u-bq898. Retrieved from <https://code.eoffice.gov.uk/trac/roses-u/browser/b/q/8/9/8/trunk>
- Medlyn, B. (1996). The optimal allocation of nitrogen within the C<sub>3</sub> photosynthetic system at elevated CO<sub>2</sub>. *Functional Plant Biology*, 23(5), 593–603. <https://doi.org/10.1071/PP9960593>
- Medlyn, B. E., Badeck, F.-W., De Pury, D. G. G., Barton, C. V. M., Broadmeadow, M., Ceulemans, R., et al. (1999). Effects of elevated [CO<sub>2</sub>] on photosynthesis in European forest species: A meta-analysis of model parameters. *Plant, Cell and Environment*, 22(12), 1475–1495. <https://doi.org/10.1046/j.1365-3040.1999.00523.x>
- Medlyn, B. E., Loustau, D., & Delzon, S. (2002). Temperature response of parameters of a biochemically based model of photosynthesis. I. Seasonal changes in mature maritime pine (*Pinus pinaster* Ait.). *Plant, Cell and Environment*, 25(9), 1155–1165. <https://doi.org/10.1046/j.1365-3040.2002.00890.x>
- Mengoli, G., Agustí-Panareda, A., Boussetta, S., Harrison, S. P., Trotta, C., & Prentice, I. C. (2022). Ecosystem photosynthesis in land-surface models: A first-principles approach incorporating acclimation. *Journal of Advances in Modeling Earth Systems*, 14(1), e2021MS002767. <https://doi.org/10.1029/2021MS002767>
- Mercado, L. M., Medlyn, B. E., Huntingford, C., Oliver, R. J., Clark, D. B., Sitch, S., et al. (2018). Large sensitivity in land carbon storage due to geographical and temporal variation in the thermal response of photosynthetic capacity. *New Phytologist*, 218(4), 1462–1477. <https://doi.org/10.1111/nph.15100>
- Oliver, R. J., Mercado, L. M., Clark, D. B., Huntingford, C., Taylor, C. M., Vidale, P. L., et al. (2022). Improved representation of plant physiology in the JULES-vn5.6 land surface model: Photosynthesis, stomatal conductance and thermal acclimation. *Geoscientific Model Development*, 15(14), 5567–5592. <https://doi.org/10.5194/gmd-15-5567-2022>
- Poulter, B., MacBean, N., Hartley, A., Khlystova, I., Arino, O., Betts, R., et al. (2015). Plant functional type classification for earth system models: Results from the European space agency's land cover climate change initiative. *Geoscientific Model Development*, 8(7), 2315–2328. <https://doi.org/10.5194/gmd-8-2315-2015>
- Reich, P. B., Sendall, K. M., Stefanski, A., Rich, R. L., Hobbie, S. E., & Montgomery, R. A. (2018). Effects of climate warming on photosynthesis in boreal tree species depend on soil moisture. *Nature*, 562(7726), 263–267. <https://doi.org/10.1038/s41586-018-0582-4>
- Ren, Y., Wang, H., Harrison, S. P., Prentice, I. C., Mengoli, G., Zhao, L., et al. (2025). Incorporating the acclimation of photosynthesis and leaf respiration in the noah-MP land surface model: Model development and evaluation. *Journal of Advances in Modeling Earth Systems*, 17(3), e2024MS004599. <https://doi.org/10.1029/2024MS004599>
- Roberts, M. J., Baker, A., Blockley, E. W., Calvert, D., Coward, A., Hewitt, H. T., et al. (2019). Description of the resolution hierarchy of the global coupled HadGEM3-GC3.1 model as used in CMIP6 HighResMIP experiments. *Geoscientific Model Development*, 12(12), 4999–5028. <https://doi.org/10.5194/gmd-12-4999-2019>
- Rogers, A., Medlyn, B. E., Dukes, J. S., Bonan, G., von Caemmerer, S., Dietze, M. C., et al. (2017). A roadmap for improving the representation of photosynthesis in Earth system models. *New Phytologist*, 213(1), 22–42. <https://doi.org/10.1111/nph.14283>
- Scafarò, A. P., Xiang, S., Long, B. M., Bahar, N. H. A., Weerasinghe, L. K., Creek, D., et al. (2017). Strong thermal acclimation of photosynthesis in tropical and temperate wet-forest tree species: The importance of altered Rubisco content. *Global Change Biology*, 23(7), 2783–2800. <https://doi.org/10.1111/gcb.13566>
- Scott, H. G., & Smith, N. G. (2022). A model of C<sub>4</sub> photosynthetic acclimation based on least-cost optimality theory suitable for Earth system model incorporation. *Journal of Advances in Modeling Earth Systems*, 14(3), e2021MS002470. <https://doi.org/10.1029/2021MS002470>
- Sellar, A. A., Jones, C. G., Mulcahy, J. P., Tang, Y., Yool, A., Wiltshire, A., et al. (2019). UKESM1: Description and evaluation of the U.K. Earth system model. *Journal of Advances in Modeling Earth Systems*, 11(12), 4513–4558. <https://doi.org/10.1029/2019MS001739>

- Sendall, K. M., Reich, P. B., Zhao, C., Jihua, H., Wei, X., Stefanski, A., et al. (2015). Acclimation of photosynthetic temperature optima of temperate and boreal tree species in response to experimental forest warming. *Global Change Biology*, 21(3), 1342–1357. <https://doi.org/10.1111/gcb.12781>
- Slot, M., & Winter, K. (2017). Photosynthetic acclimation to warming in tropical forest tree seedlings. *Journal of Experimental Botany*, 68(9), 2275–2284. <https://doi.org/10.1093/jxb/erx071>
- Smith, N. G., & Dukes, J. S. (2017). Short-term acclimation to warmer temperatures accelerates leaf carbon exchange processes across plant types. *Global Change Biology*, 23(11), 4840–4853. <https://doi.org/10.1111/gcb.13735>
- Smith, N. G., & Keenan, T. F. (2020). Mechanisms underlying leaf photosynthetic acclimation to warming and elevated CO<sub>2</sub> as inferred from least-cost optimality theory. *Global Change Biology*, 26(9), 5202–5216. <https://doi.org/10.1111/gcb.15212>
- Smith, N. G., Malyshev, S. L., Shevliakova, E., Kattge, J., & Dukes, J. S. (2016). Foliar temperature acclimation reduces simulated carbon sensitivity to climate. *Nature Climate Change*, 6(4), 407–411. <https://doi.org/10.1038/nclimate2878>
- Smith, N. G., Zhu, Q., Keenan, T. F., & Riley, W. J. (2024). Acclimation of photosynthesis to CO<sub>2</sub> increases ecosystem carbon storage due to leaf nitrogen savings. *Global Change Biology*, 30(11), e17558. <https://doi.org/10.1111/gcb.17558>
- Terrer, C., Jackson, R. B., Prentice, I. C., Keenan, T. F., Kaiser, C., Vicca, S., et al. (2019). Nitrogen and phosphorus constrain the CO<sub>2</sub> fertilization of global plant biomass. *Nature Climate Change*, 9(9), 684–689. <https://doi.org/10.1038/s41558-019-0545-2>
- Vårhammar, A., Wallin, G., McLean, C. M., Dusenke, M. E., Medlyn, B. E., Hasper, T. B., et al. (2015). Photosynthetic temperature responses of tree species in Rwanda: Evidence of pronounced negative effects of high temperature in montane rainforest climax species. *New Phytologist*, 206(3), 1000–1012. <https://doi.org/10.1111/nph.13291>
- Walker, A. P., Beckerman, A. P., Gu, L., Kattge, J., Cernusak, L. A., Domingues, T. F., et al. (2014). The relationship of leaf photosynthetic traits – V<sub>cmax</sub> and J<sub>max</sub> – To leaf nitrogen, leaf phosphorus, and specific leaf area: A meta-analysis and modeling study. *Ecology and Evolution*, 4(16), 3218–3235. <https://doi.org/10.1002/ece3.1173>
- Wang, Z., & Wang, C. (2021). Magnitude and mechanisms of nitrogen-mediated responses of tree biomass production to elevated CO<sub>2</sub>: A global synthesis. *Journal of Ecology*, 109(12), 4038–4055. <https://doi.org/10.1111/1365-2745.13774>
- Warren, J. M., Jensen, A. M., Medlyn, B. E., Norby, R. J., & Tissue, D. T. (2015). Carbon dioxide stimulation of photosynthesis in Liquidambar styraciflua is not sustained during a 12-year field experiment. *AoB Plants*, 7. <https://doi.org/10.1093/aobpla/plu074>
- Wieder, W. R., Cleveland, C. C., Smith, W. K., & Todd-Brown, K. (2015). Future productivity and carbon storage limited by terrestrial nutrient availability. *Nature Geoscience*, 8(6), 441–444. <https://doi.org/10.1038/ngeo2413>
- Williams, K. D., Copsey, D., Blockley, E. W., Bodas-Salcedo, A., Calvert, D., Comer, R., et al. (2018). The Met office global coupled model 3.0 and 3.1 (GC3.0 and GC3.1) configurations. *Journal of Advances in Modeling Earth Systems*, 10(2), 357–380. <https://doi.org/10.1002/2017MS001115>
- Wiltshire, A. J., Duran Rojas, M. C., Edwards, J. M., Gedney, N., Harper, A. B., Hartley, A. J., et al. (2020). JULES-GL7: The global land configuration of the joint UK land environment simulator version 7.0 and 7.2. *Geoscientific Model Development*, 13(2), 483–505. <https://doi.org/10.5194/gmd-13-483-2020>
- Xiao, Z., Liang, S., Wang, J., Xiang, Y., Zhao, X., & Song, J. (2016). Long-time-series global land surface satellite leaf area index product derived from MODIS and AVHRR surface reflectance. *IEEE Transactions on Geoscience and Remote Sensing*, 54(9), 5301–5318. <https://doi.org/10.1109/TGRS.2016.2560522>
- Yamori, W., Hikosaka, K., & Way, D. A. (2014). Temperature response of photosynthesis in C3, C4, and CAM plants: Temperature acclimation and temperature adaptation. *Photosynthesis Research*, 119(1), 101–117. <https://doi.org/10.1007/s11120-013-9874-6>
- Yang, J., Medlyn, B. E., De Kauwe, M. G., Duursma, R. A., Jiang, M., Kumarathunge, D., et al. (2020). Low sensitivity of gross primary production to elevated CO<sub>2</sub> in a mature eucalypt woodland. *Biogeosciences*, 17(2), 265–279. <https://doi.org/10.5194/bg-17-265-2020>